REPORT DOCUMENTATION PAGE

Form Approved
OMB No. 0704-0188

1. REPORT DATE *(DD-MM-YYYY)*	**2. REPORT TYPE**	**3. DATES COVERED** *(From - To)*
July 2015	Technical Paper	July 2015-July 2015

4. TITLE AND SUBTITLE
Comparison of Laminar and Linear Eddy Model Closures for Combustion Instability Simulations

5a. CONTRACT NUMBER
In-House

5b. GRANT NUMBER

5c. PROGRAM ELEMENT NUMBER

6. AUTHOR(S)
Harvazinski, M., Talley, D., Sankran, V.

5d. PROJECT NUMBER

5e. TASK NUMBER

5f. WORK UNIT NUMBER
Q0A1

7. PERFORMING ORGANIZATION NAME(S) AND ADDRESS(ES)

Air Force Research Laboratory (AFMC)
AFRL/RQRC
10 E. Saturn Blvd.
Edwards AFB, CA93524-7680

8. PERFORMING ORGANIZATION REPORT NO.

9. SPONSORING / MONITORING AGENCY NAME(S) AND ADDRESS(ES)
Air Force Research Laboratory (AFMC)
AFRL/RQR
5 Pollux Drive
Edwards AFB CA 93524-7048

10. SPONSOR/MONITOR'S ACRONYM(S)

11. SPONSOR/MONITOR'S REPORT NUMBER(S)
AFRL-RQ-ED-TP-2015-274

12. DISTRIBUTION / AVAILABILITY STATEMENT
Distribution A: Approved for Public Release; Distribution Unlimited.

13. SUPPLEMENTARY NOTES
Technical Paper and Briefing Charts presented at AIAA Propulsion and Energy; Orlando, FL; July 29, 2015. PA#15382.

14. ABSTRACT
Unstable liquid rocket engines can produce highly complex dynamic flowfields with features such as rapid changes in temperature and pressure, increased heat transfer, local flame extinction and reignition, and local partially-premixed and non-premixed combustion.
This type of flowfield represents a challenge for turbulent combustion models, which are typically associated with a number of assumptions that limit regime applicability. In the present study, the linear eddy model (LEM) is applied to an unstable single element liquid rocket engine to assess its performance and to contrast it with simple laminar combustion model (LCM). Two distinct operating conditions showing different dynamic behavior are used; the first is marginally stable and has peak-to-peak amplitudes of 12% of the mean, while the second is strongly unstable and has pressure amplitudes in excess of 40% of the mean. Results show that while the LEM is able to capture the general dynamics behavior, the trends are in the wrong direction when compared with the experimental results. In other words, the stable case becomes more unstable and the unstable case becomes more stable. The paper also examines the underlying assumptions of the LEM and suggests reasons for the observed behavior.

15. SUBJECT TERMS

16. SECURITY CLASSIFICATION OF:			**17. LIMITATION OF ABSTRACT**	**18. NUMBER OF PAGES**	**19a. NAME OF RESPONSIBLE PERSON**
					Doug Talley
a. REPORT	**b. ABSTRACT**	**c. THIS PAGE**	SAR	53	**19b. TELEPHONE NO** *(include area code)*
Unclassified	**Unclassified**	**Unclassified**			661-275-6174

Standard Form 298 (Rev. 8-98)
Prescribed by ANSI Std. 239.18

Comparison of Laminar and Linear Eddy Model Closures for Combustion Instability Simulations

Matthew E. Harvazinski*, Douglas G. Talley†, and Venkateswaran Sankaran‡
Air Force Research Laboratory, Edwards AFB, CA, 93524

Unstable liquid rocket engines can produce highly complex dynamic flowfields with features such as rapid changes in temperature and pressure, increased heat transfer, local flame extinction and reignition, and local partially-premixed and non-premixed combustion. This type of flowfield represents a challenge for turbulent combustion models, which are typically associated with a number of assumptions that limit regime applicability. In the present study, the linear eddy model (LEM) is applied to an unstable single element liquid rocket engine to assess its performance and to contrast it with simple laminar combustion model (LCM). Two distinct operating conditions showing different dynamic behavior are used; the first is marginally stable and has peak-to-peak amplitudes of 12% of the mean, while the second is strongly unstable and has pressure amplitudes in excess of 40% of the mean. Results show that while the LEM is able to capture the general dynamics behavior, the trends are in the wrong direction when compared with the experimental results. In other words, the stable case becomes more unstable and the unstable case becomes more stable. The paper also examines the underlying assumptions of the LEM and suggests reasons for the observed behavior.

Nomenclature

A	Mode amplitude
c_p	Constant pressure specific heat capacity
f	Frequency
F_{stir}	LEM stirring model
p	Pressure
$\widetilde{P}$	Joint-PDF
T	Temperature
V_k	Diffusion velocity
Y_k	Species mass fraction
$\Delta h^\circ_{f,k}$	Enthalpy of formation
λ	Thermal conductivity
μ	Viscosity
ρ	Density
$\dot{\omega}$	Species production
$\tilde{\dot{\omega}}$	Filtered species production
LCM	Laminar combustion model
LEM	Linear eddy model

I. Introduction

Combustion instabilities have plagued rocket engine development since the 1950s. Lacking a truly predictive model, combustion instability remains a large risk in the design and acquisition of new hardware.

*Research Aerospace Engineer, AIAA Member.
†Principal Research Physical Scientist, AIAA Associate Fellow.
‡Senior Scientist, AIAA Senior Member.

Recently, large eddy simulations (LES) of reacting flow have made it possible to capture unstable behavior observed in laboratory scale experiments.[1–3] One of the challenges of using LES to simulate turbulent reacting flow is the closure of the filtered species production term. In the laminar combustion mode (LCM), the filtered production term is simply taken to be the reaction rates evaluated using the filtered flow variables,

$$\widetilde{\dot{\omega}} = \dot{\omega}\left(\widetilde{T}, \widetilde{Y_k}\right) \tag{1}$$

A more appropriate turbulent closure would invoke the joint probability density function to define the turbulent combustion source term,

$$\widetilde{\dot{\omega}} = \int_{T_{\min}}^{T_{\max}} \int_0^1 \dot{\omega}\left(Y_k, T\right) \widetilde{P}\left(Y_k, T; \mathbf{x}, t\right) \mathrm{d}Y_k \, \mathrm{d}T \tag{2}$$

Where $\widetilde{P}$ is the joint-PDF of the species mass fractions and temperatures and needs to be computed or specified. Numerous approaches have been proposed in the literature for this purpose; possible options include flamelets,[4] transported PDF,[5,6] linear eddy model (LEM),[7] and the dynamically thickened flame (DTF) model.[8] The difficulty is that none of these closures is applicable to a wide range of combustion regimes and operating conditions. This is especially true for combustion instability predictions which involve investigating off-design conditions where complex combustion dynamics phenomena such as flame blowout, ignition, extinction, acoustic interaction, and transient events can occur.

Many of these models have fundamental assumptions such as constant pressure, incompressible low speed flow, and unity Lewis numbers, which are not applicable to Air Force propulsion systems including liquid rocket engines. Flamelets assume that the flame is very thin and are valid for low Mach low Reynolds number flows and rely on a presumed PDF to close the turbulence. The transported PDF model is an attractive alternative because the joint-PDF is computed (i.e., not assumed) and the filtered source term can be computed directly. The drawback of this model is that the mixing is not directly captured and an auxiliary mixing model must be used, which remains a serious challenge. Moreover, the general formulation of joint-PDF velocity, composition, temperature, pressure and turbulent frequency has not been clearly demonstrated for the problems of interest here.[9]

On the other hand, the linear eddy model is a genuine multi-scale model that augments the governing equations for the resolved scales with a 1d model equation system for the sub-grid scales.[7] The cornerstone of the sub-grid model is the introduction of a stirring term that models the sub-grid mixing under the assumption of certain statistical behavior. The advantage of the approach is that there are no assumptions made of the nature of the combustion and the mixing model impacts only the sub-grid closure. Because application of the LEM is the focus of the paper, a more detailed description of the model is given in the next section along with detailed critique of the underlying assumptions and their possible impacts on the solution.

The specific objective of the current study is to compare the performance of the LEM closure model with the standard LCM closure for the prediction of combustion instabilities in a single-element gaseous rocket engine. In the experiments (see background), the length of the shear-coaxial injector post is systematically altered to trigger longitudinal instabilities in the combustion chamber.[10] Two specific operating conditions are selected that show discriminatory behavior experimentally—in other words, one post-length condition leads to marginally stable/unstable operation, while the second post-length condition is observed to be highly unstable. Previous computational studies using detached eddy simulations (DES) with laminar combustion closure have demonstrated the ability to predict the discriminatory behavior qualitatively, but not the quantitative magnitudes of the amplitudes and frequencies. In this paper, we assess the ability of the LEM to predict the instability amplitudes and their frequencies and contrast them with the laminar closure results.

The paper is organized as follows. First, the LEM is reviewed along with a critique of the underlying assumptions of the model. This is followed by descriptions of the experimental configuration and previous attempts to model the problem using the simple LCM closure. In the next section, we provide details of the present simulations. Next, in the results section, we compare and contrast the LEM and laminar closure models for the two operating conditions. In particular, detailed flowfield visualizations are used to examine the prediction differences and assess the relative performance of the LEM. The final section provides a summary of the results and model abilities.

II. The Linear Eddy Model

The linear eddy model is described in detail in Kerstein,[7] Menon et al.[11,12] In this model, each 3D LES cell has a one-dimensional LEM grid with a grid resolution commensurate with the Kolmogorov scale. On the LEM grid, a modified set of 1D conservation equations are solved for the species mass fraction and the energy which take the form,

$$\frac{\partial Y_k}{\partial t} = F_{k,\text{stir}} - \frac{1}{\rho}\frac{\partial}{\partial s}\left(\rho Y_k V_k\right) + \frac{\dot{\omega}_k}{\rho} \tag{3}$$

$$\frac{\partial T}{\partial t} = F_{T,\text{stir}} - \frac{1}{c_p}\sum_{k=1}^{N} c_{p,k} Y_k V_k \frac{\partial T}{\partial s} + \frac{1}{\rho c_p}\frac{\partial}{\partial s}\left(\lambda \frac{\partial T}{\partial s}\right) + \frac{1}{\rho c_p}\sum_{k=1}^{N} \Delta h^{\circ}_{f,k}\dot{\omega}_k \tag{4}$$

In the energy equation, it is assumed that c_p is a function of the temperature only and that the sub-grid pressure is a constant and equal to the resolved scale pressure. The diffusion velocities are modeled using the typical Fickian approximation. Both conservation equations include a stirring term, F_{stir}. This term is used to simulate the effect of an eddy in the sub-grid by stirring the profile. This process is shown pictorially in Figure 1. To stir the profile, the profile is compressed to one third of the length, copied twice with the middle section reversed to conserve mass and energy. The size, location, and frequency of the eddy are specified based on observed turbulent statistics.[12] In practice, Eqns. 3 and 4 are evolved in time at each LES time step with the stirring and diffusion events occurring at prescribed intervals.

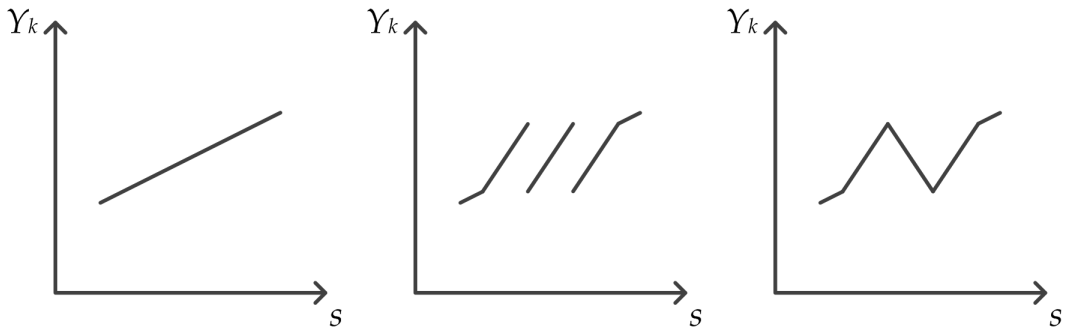

Figure 1: Cartoon of the stirring event, the image on the left is the original profile; the center image shows the profile being replicated twice while its length is reduced by a factor of three, in the final image on the right the middle segment is mirrored to ensure mass conservation. This gives the effect of a one-dimensional eddy moving through the field. The same technique is also applied to the sub-grid temperature profile.

A criticism of the linear eddy model is that it is not strictly a sub-grid model. The conservation equations for the filtered species in the resolved scale are not solved in their conventional Eulerian form. Instead, the species solutions in the sub-grid are transported between LES cells using a so-called Lagrangian splicing model. To accomplish this, each LEM grid is assigned an input end and an output end. Mass exiting the LES cell is extracted from the output end and mass entering the LES cell is added to the input end. The movement of the mass is done based on the direction and magnitude of the convective fluxes at the LES cell faces but the selection of which LEM cells move to which neighboring cells is arbitrary. The advantage of this approach is that co-gradient and counter-gradient sub-grid structures are accounted for which would be absent in a standard gradient diffusion approach.[12] A further limitation of such an implementation is that species mass diffusion in the resolved scale is not accounted for. Thus, as the grid spacing approaches the DNS limit, the model becomes invalid because of the absence of diffusion between the LES cells. Another difficulty of the LEM model is the presence of two temperatures, a resolved scale filtered temperature and the approximate sub-grid scale temperature which raises the question as to how well coupled are the sub-grid and resolved grid energy transfers.

III. Background

The present study models the continuously variable resonance combustor (CVRC) experiment. The CVRC is a laboratory scale single element gas centered shear coax injector, which has shown varying levels of

longitudinal instability. The amplitude of the instability is varied by adjusting the length of the oxidizer post. Both marginally stable and unstable conditions have been realized. The CVRC is an excellent experiment to model because of its complex physics and wide range of behavior spanned by a single parameter (the oxidizer post length). This allows for an evaluation of models model under widely different conditions for a nearly constant set of parameters. Two specific test configurations are adopted in the present study, one of which is marginally stable and the second that is highly unstable. For the marginally stable case, the peak-to-peak pressure fluctuations are observed experimentally to be 12% of the mean, while in the unstable configuration, the peak-to-peak amplitudes exceed 40% of the mean.[10]

Prior simulations by Harvazinski et al. used a DES based approach with LCM closure and found excellent qualitative agreement with the data.[1] Garby et al. used a LES solver with a dynamically thickened flame (DTF) for the turbulent combustion closure.[3] Srinivasan et al. also used LES but with the LEM closure.[2] A summary of the operating conditions and results are shown in Table 1. Here, the 8.89 cm post-length case corresponds to the marginally stable operation, while the 13.97 cm case corresponds to the highly unstable condition. The longer post-length of 19 cm gave somewhat unrepeatable experimental results, which were sometimes observed to be stable and sometimes unstable. For this reason, this case was not chosen for the present study. The ratios of the simulation to experimental data for the first mode frequency and amplitudes are also reported in the table. Each modeling approach over-predicted the frequency compared to the experiment. Direct comparisons to assess the effect of the turbulent combustion closure are not possible because of differences in turbulence models, grids, and numerical methods, but it is noteworthy that the LEM predictions of Srinivasan et al. over-predict the amplitudes of the marginally stable case (9 cm) and under-predict the amplitudes of the most unstable case (14 cm).

Table 1: Simulation results.

	Harvazinski et al.[1]	Srinivasan et al.[2]	Garby et al.[3]
Code	GEMS	LESLIE3D	AVBP
Turbulence Model	DES	LES	LES
Combustion Closure	Laminar	LEM	DTF
Grid Size	5 M	1.4 M	14 M
Post Lengths, cm	8.89, 13.97, 19.05	9.0, 12.0, 14.0	12.0
$f_1/f_{1,\text{exp}}$	1.24, 1.16, 1.18	1.2, 1.16, 1.19	1.09
$A_1/A_{1,\text{exp}}$	1.07, 0.90, 1.93	4.34, 0.34, 0.47	Not Reported

The previous studies have also identified a complex triple flame structure, which represents the intersection of a leading fuel rich premixed flame, leading fuel lean premixed flame and a trailing diffusion flame. This structure is shown in Figure 2 for the 13.97 cm post-length configuration and was captured using the LCM closure.[1,13] Similar results have been predicted with the DTF model.[3] In both cases, this structure is highly dynamic and moves from the cup region in the injector post to the combustor during the course of a cycle. It has been observed that, in the marginally stable case (not shown), the triple flame does not enter the cup region and the flame remains anchored to the injector face in the combustor dump-plane.

In addition to the presence of the unsteady triple flame structure, the main source of the instability in the 13.97 cm configuration is the coupling between the acoustics and heat release. The heat release is cyclic over the period of the first longitudinal acoustic mode and occurs as the result of a temporary interruption in the fuel supply into the combustor. Figure 3 shows this fuel disruption event and the subsequent re-ignition event. The fuel supply is disrupted in the cup region by the pressure pulse moving from the combustor upstream into the oxidizer post. There is increased mixing in this area which also leads to combustion taking place. The combination of the fuel being pushed backward and the combustion leads to a cutoff in the supply of fuel into the combustor. This allows the combustion zone in the combustor to move downstream, away from the head-end of the combustor. As the fuel reenters the combustor it does so without burning. The unburned methane accumulates in the shear layer and eventually re-ignites when the oxidizer post pressure wave returns to the head end of the combustor. This reflected pressure wave pushes the accumulated methane into the warmer recirculating gases causing ignition to takes place. In the unstable case, this is so timed that the returning pressure wave in the combustor ,further amplifies the combustion and sets up the fuel

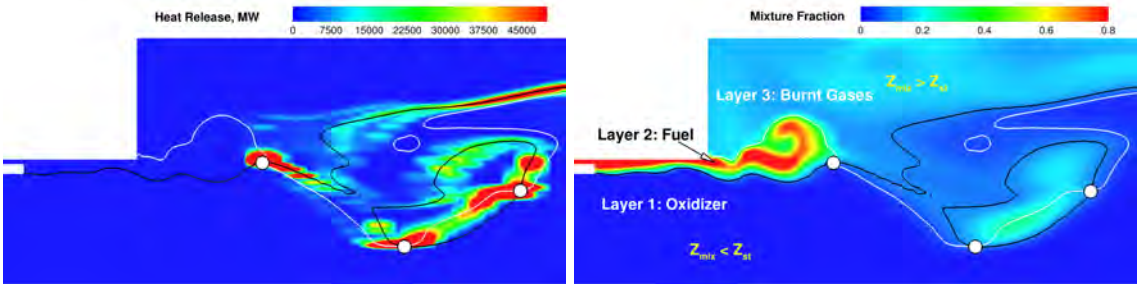

Figure 2: Triple Flame structure, three triple points are identified (white circles) at the intersection of the white and black lines. In both plots the white line is a $T = 2000\,\mathrm{K}$ contour and the black line is the stoichiometric mixture fraction, Z_{st}.

cutoff event for the next cycle. In the marginal stable case the length of the oxidizer post is shorter and does not allow for a strong coupling between the waves in the oxidizer post and the combustor. This results in heat release that is more-or-less continuous throughout the cycle and there is no disruption event and no combustion in the cup region. In fact, as noted earlier, the flame remains anchored to the dump plane throughout the acoustic cycle and thus displays very different dynamics when compared to the unstable case. These two distinct operating points therefore serve as excellent test cases for model validation and are utilized here to contract the performance of the LCM and LEM closures.

(a) Fuel disruption.

(b) Re-ignition event.

Figure 3: Key events in the CVRC instability mechanism. In both figures the red is unburnt fuel, the yellow is combustion and the green is the oxidizer pressure pulse. In (a) the oxidizer pressure pulse is moving from the combustor into the oxidizer post, when it passes by the fuel it creates a temporary stoppage in the supply. Increased mixing due to the baroclinic torque leads to combustion in the cup region. For the reignition shown in (b) the oxidizer pressure pulse travels from the oxidizer post into the combustor, in doing so it pushes unburnt fuel into the warm recirculating gases near the dump plane which leads to combustion and a rapid burning of the unburnt accumulated fuel.

IV. Simulation Details

Two different oxidizer post lengths are simulated to evaluate the LEM and to contrast it with the previously-obtained LCM results. The corresponding oxidizer post lengths are 8.89 cm and 13.97 cm, which correspond to the marginally stable and unstable operating points respectively. All other operating parameters remain the same for all of the simulations and are summarized in Table 2.

The simulations are run using LESLIE3D developed at Georgia Tech.[14–17] LESLIE3D is a compressible LES solver, which uses a hybrid second-order central and third-order MUSCL scheme. An additional transport equation for k_{sgs} is solved to close the momentum and energy equations. Both the laminar and LEM closure are used along with a two-step reduced chemical kinetics mechanism,

$$\mathrm{CH_4} + \tfrac{3}{2}\mathrm{O_2} \longrightarrow \mathrm{CO} + 2\,\mathrm{H_2O} \tag{5}$$

$$\mathrm{CO} + \tfrac{1}{2}\mathrm{O_2} \longleftrightarrow \mathrm{CO_2} \tag{6}$$

Table 2: Operating conditions.

Parameter	Value
Oxidizer Composition	57.6% H_2O, 42.4% O_2
Oxidizer temperature, K	1030
Oxidizer flow rate, kg/s	0.320
Fuel Composition	100% CH_4
Fuel temperature, K	300
Fuel flow rate, kg/s	0.027
Nozzle back pressure, kPa	101.325

The mechanism is due to Franzelli et al. and supplements the global reaction with an equilibrium reaction to balance the concentrations of CO and CO_2.[18] Constant mass flow boundaries are used to supply the oxidizer and fuel to the domain. There is a choked nozzle located at the downstream end of the combustor and the walls are adiabatic. A sketch of the computational domain is shown in Figure 4. Two multi-block structured meshes were generated, one for each of the oxidizer post lengths. The meshes are nearly identical differing only in the length of the oxidizer post. The resolution in the oxidizer post is the same for both cases, which results in mesh sizes of 8.6 M and 8.9 M for the short and long lengths respectively.

For the initial condition the oxidizer post is filled with oxidizer at a constant temperature of 1030 K and the fuel annulus is filled with methane at 300 K. The remainder of the combustor is filled with a mix of H_2O and CO_2 at 1500 K, which allows the methane to auto-ignite rapidly. Prior work has shown the final limit cycle amplitude to be insensitive to the initial temperature of the combustor. Simulations are then run for a total of 40 ms. The LEM closure requires an initial reacting flow solution to initialize, to accomplish this; therefore, the first 3 ms of the LEM simulations are run using the laminar closure after which the LEM is activated. For the LEM simulation 12 LEM cells are used per LES cell which gives a resolution commensurate with the Kolmogorov scale in the shear layer region of the mesh. The pressure at the several wall locations corresponding to experimental transducer locations are recorded every time-step, while the full three-dimensional flowfield is saved every 0.01 ms.

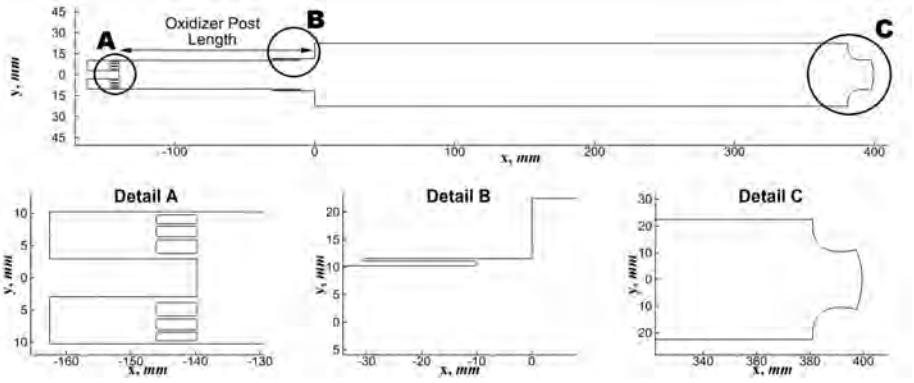

Figure 4: Computational domain.

V. Results

In this section, we examine the predicted results for the two oxidizer post-length cases using the LESLIE3D code with LCM and LEM closures. We begin by considering the pressure time histories followed by power spectral density analysis to elucidate the modal content in the results. We then examine the detailed combustion dynamics as a function of the acoustic wave period for each case to discern the underlying mechanisms predicted by the two models. Importantly, we address the reasons for the predictive trends in the frequency and amplitudes of the dominant modes.

A. Pressure Time History

The temporal evolution of the unsteady pressure is shown in Figure 5 along with a 10 ms snapshot showing the fluctuating pressure for each of the simulations. Examination of the pressure signals shows that both the LCM and LEM closures are able to capture the discriminating amplitudes of the marginally stable and unstable operating point. However, the choice of combustion closure impacts the predicted pressure amplitudes and mean pressure. From the fluctuating pressure signal, it is clear that the amplitude predicted using the LEM closure is higher for the marginally stable operating point and lower for the unstable operating point compared with the laminar closure. In addition to differences in the pressure amplitude, the mean pressure is also shifted lower for both LEM cases. The LCM cases are 1.69 MPa and 1.68 MPa, while the LEM cases are 1.61 MPa and 1.60 MPa for the unstable and marginally stable operating conditions respectively. The experimental operating pressure is approximately 1.3 MPa.[19] It is believed that the over prediction in the mean pressure is the result of the adiabatic wall boundary condition which leads to higher total temperatures and pressures in the combustor.[20] The lower mean pressure predicted by LEM is indeed the correct qualitative trend, although since sets of calculations use the adiabatic wall temperature, it is possible that the LEM results indicate incomplete combustion.

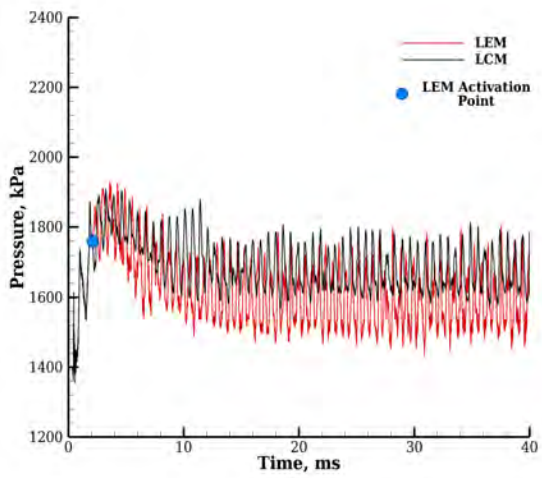

(a) Marginally stable

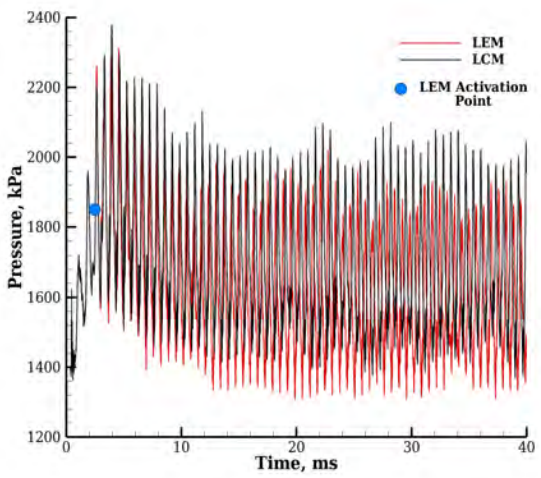

(b) Unstable

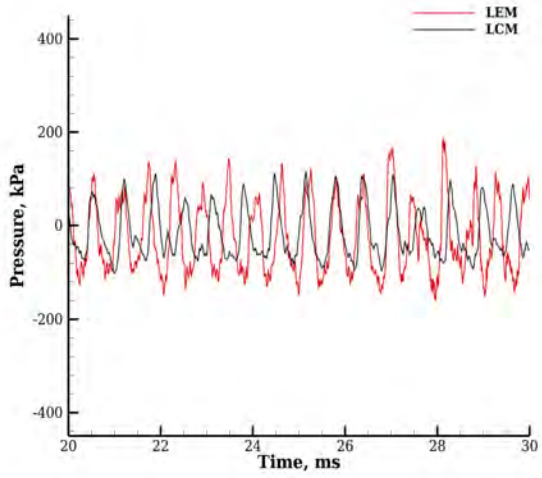

(c) Marginally stable

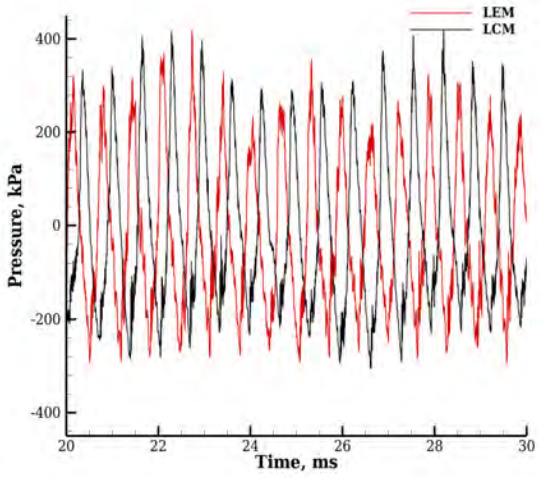

(d) Unstable

Figure 5: Pressure trace for the marginally stable and unstable conditions. Sub-figures (a) and (b) show the full time history of the unsteady pressure and sub-figures (c) and (d) show a 10 ms snapshot of the fluctuating pressure. The point which the LEM closure is activated is marked in the time history.

B. Power Spectral Density Analysis

A power spectral density (PSD) analysis is performed to analyze the frequency content and amplitude of the individual modes. The PSDs are generated using the final 35 ms of data, providing a frequency resolution of ± 28.57 Hz. An explicit time marching algorithm is used which results in a variable sample rate of the pressure. To perform the PSD analysis, the pressure time history is first interpolated onto a 1×10^{-7} s uniformly spaced temporal grid. This provides a maximum frequency of 5 MHz, which is well above the frequencies of interest in the current study. The PSD plots for the four cases along with the experimental results are shown in Figure 6. For the unstable operating point, both models capture the high-amplitude well-defined harmonics for the first 3 modes. With the LEM closure, the fourth and fifth modes show a bifurcation. The experimental data and LCM simulation do not exhibit such a bifurcation. The marginally stable operating point has a well-defined first mode and a lower amplitude second mode. Both closures capture this but they tend to overpredict the amplitude of the second mode. The over prediction of the second mode has been seen in other computational work using an unstructured-DES code as well.[1]

More quantitative data concerning the amplitudes and frequency are presented in Tables 3 and 4, which tabulate the frequency and amplitude for the first several modes for the two operating points. The amplitudes are computed by integrating under the PSD peaks using a full-width half-max approach that is consistent with the experimental data reduction procedure.[10] Similar to the prior studies of this experiment, the current frequency predictions are larger than the experiment.[1–3] This is likely due to a combination of the global kinetics and the adiabatic wall boundary condition, both of which contribute to a higher combustor temperature and concomitantly a larger value of the predicted sound speed in the combustor. The overall amplitudes (sum of the first three modes) for the marginally stable operating point are over predicted by both models–i.e., by 1.4% and 41.0% for the LCM and LEM closures respectively. We note that this is a significant difference since the LCM closure provides closer agreement with the experimental data than the more advanced LEM closure. On the other hand, the amplitude predictions of the 1L mode for the highly unstable case are lower than the experimental value by 11.3% and 19.6% for the laminar and LEM closures respectively. This represents better agreement although the LEM result is once again indicating a counter-trend. In other words, the trend for the LEM closure is in the wrong direction for both cases–i.e., the stable case becomes more unstable and the unstable case becomes more stable compared with the LCM simulations.

Predictions of the harmonic nature of the instability are also different between the LEM and LCM closures. It is expected that the ratio of the higher order mode frequency to the first mode frequency would be integer multiples. For the highly unstable case, this is observed experimentally up to the fourth mode, and both closure models predict this reasonably well. For the marginally stable case, this relationship between harmonics is more difficult to establish because of the lower energy content in the higher harmonics. Experimentally for this case, only the second mode is observed to be an integer multiple of the first mode. Again, this harmonic relationship is correctly predicted by the LCM closure but not with the LEM which predicts the ratio of the first and second mode frequencies to be 1.59. Also, for the marginally stable case, the third mode occurs at 2.82 times the fundamental frequency in the experiments, while both closures predict somewhat lower values. Table 5 shows a comparison of the first mode amplitudes and frequencies to the experimental data. Compared to the results of Srinivasan et al. the current work shows better amplitude predictions for both cases. Frequency predictions are slightly better for the unstable and slightly worse for the marginally stable compared to Srinivasan et al., see Table 1.

Table 3: Marginally stable PSD results showing the amplitude and frequency for the experiment and the two simulations.

Mode	Experiment			LCM			LEM		
	f, Hz	p'_{ptp}, kPa	f_i/f_1	f, Hz	p'_{ptp}, kPa	f_i/f_1	f, Hz	p'_{ptp}, kPa	f_i/f_1
1	1379	121.70	1.00	1536	95.50	1.00	1710	146.63	1.00
2	2734	5.86	1.98	3072	36.89	2.00	2725	34.00	1.59
3	3882	16.03	2.82	4232	12.71	2.76	4203	21.12	2.46
Total		143.06			145.10			201.75	

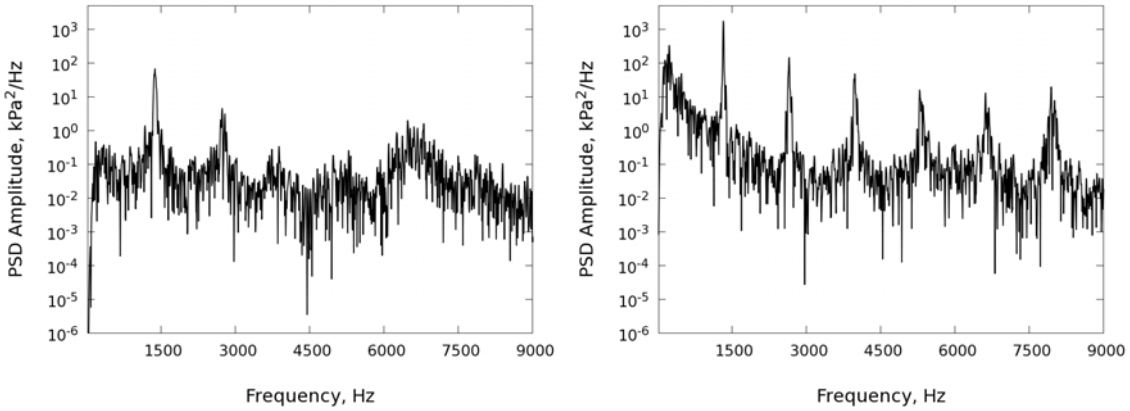

(a) Experiment - marginally stable

(b) Experiment - unstable

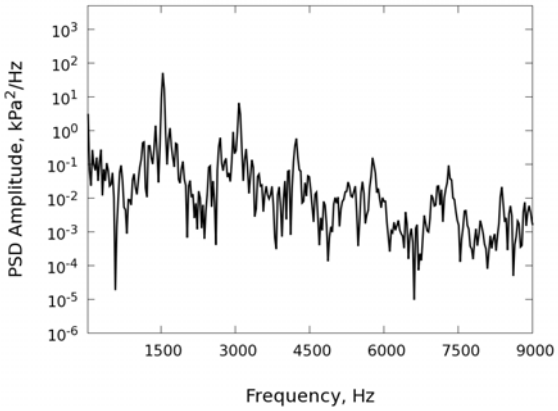

(c) LCM closure - marginally stable

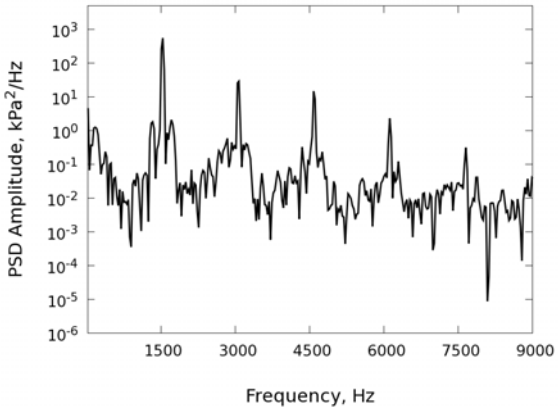

(d) LCM closure - unstable

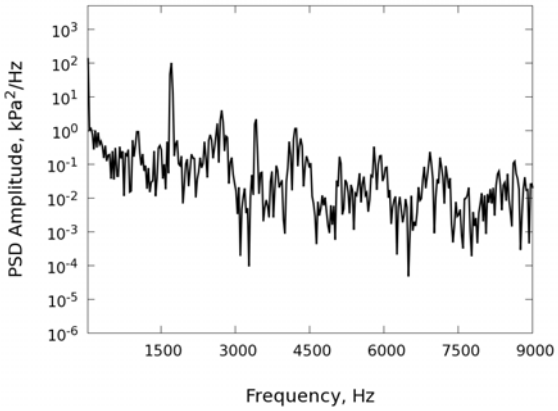

(e) LEM closure - marginally stable

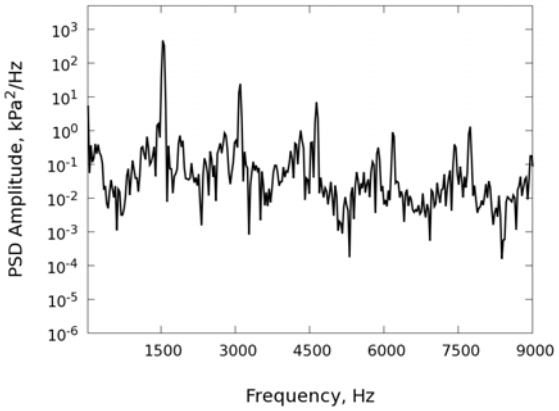

(f) LEM closure - unstable

Figure 6: Power spectral density (PSD) plots for the experiment and four simulations, left column is the marginally stable results and the right column is the unstable results. Period of analysis is the final 35 ms of the simulation

Table 4: Unstable PSD results showing the amplitude and frequency for the experiment and the two simulations.

Mode	Experiment			LCM			LEM		
	f, Hz	p'_{ptp}, kPa	f_i/f_1	f, Hz	p'_{ptp}, kPa	f_i/f_1	f, Hz	p'_{ptp}, kPa	f_i/f_1
1	1324	387.15	1.00	1536	337.42	1.00	1536	333.22	1.00
2	2655	89.29	2.01	3073	89.27	2.00	3101	69.78	2.02
3	3979	46.37	3.01	4580	54.77	2.98	4638	36.15	3.02
4	5296	41.97	4.00	6116	19.62	3.98	6174	14.90	4.02
Total		564.78			501.08			454.05	

Table 5: First mode comparisons to the experimental results.

Case	$f_1/f_{1,\text{exp}}$	$A_1/A_{1,\text{exp}}$
Marginally Stable, LCM	1.11	0.780
Marginally Stable, LEM	1.24	1.20
Unstable, LCM	1.16	0.872
Unstable, LEM	1.16	0.861

C. Dynamics of the Marginally Stable Operating Point

The more significant discrepancy in the LCM and LEM predictions is in the marginally stable operation. Figure 7 shows the temperate at the high and low pressure points of a representative cycle. A cycle starts with the pressure at the combustor head-end at a local maximum, continues as the head-end pressure deceases to a local minimum and ends with the head-end pressure returning to a local maximum. The flowfield for the LCM closure shows more intricate interfaces between the oxidizer and burnt gases consistent with roll-up from the dump plane edge. On the other hand, the LEM flowfield has smoother flow features. The acoustic wave length is much larger than any of these characteristic structures and it is possible that the acoustics are insensitive to these smaller differences. At the high pressure point, the penetration distance of the oxidizer is shorter with the LEM, indicating more complete and rapid combustion, which in turn suggests that higher heat release may be occurring near the head-end. Alternately, at the low pressure point, the oxidizer penetration distance is greater for the LEM closure than the LCM closure, which indicates slower heat release in the LEM case. Importantly, these results show that the LCM solution is more uniform during the cycle, while the LEM flowfield show a greater degree of pressure coupling, an aspect that would explain the higher pressure amplitudes observed in the LEM results. We further note that the temperature in the recirculation region is also lower for the LEM solution compared with the LCM solution (2500 K compared with 2850 K), which is consistent with the lower mean pressure observed.

The temporal evolution of the heat release for a single cycle is shown in Figure 8. Similar to the temperature flowfield shown previously the temporal evolution of the LCM closure shows significant roll up and mixing in the shear layer between the oxidizer and the recirculation region. This is evident by the stoichiometric mixture fraction iso-line and the 2000 K isotherm. The LCM closure predicts the isotherm and mixture fraction line to be very close to each other in the vicinity of the dump plane while the LEM simulation shows a significant separation between the two. Importantly, both solutions show the flame to be anchored at the dump-plane throughout the cycle, a feature that characterizes stable behavior. Both solutions also predict that the majority of the heat release takes place away from the dump plane. The LEM heat release, however, is concentrated in specific regions while the laminar model shows a more distributed heat release. Indeed, the heat release contours confirm that the LEM case is more strongly coupled with the chamber acoustics than the LCM case. In other words, for the LEM case, the first snapshot, which corresponds to the pressure maxima at the combustor head-end, shows strong heat release, while the third snapshot, which corresponds to the local pressure minima, shows diminished heat release. This stronger coupling of the heat release with the acoustic modes is no doubt responsible for the high pressure amplitudes

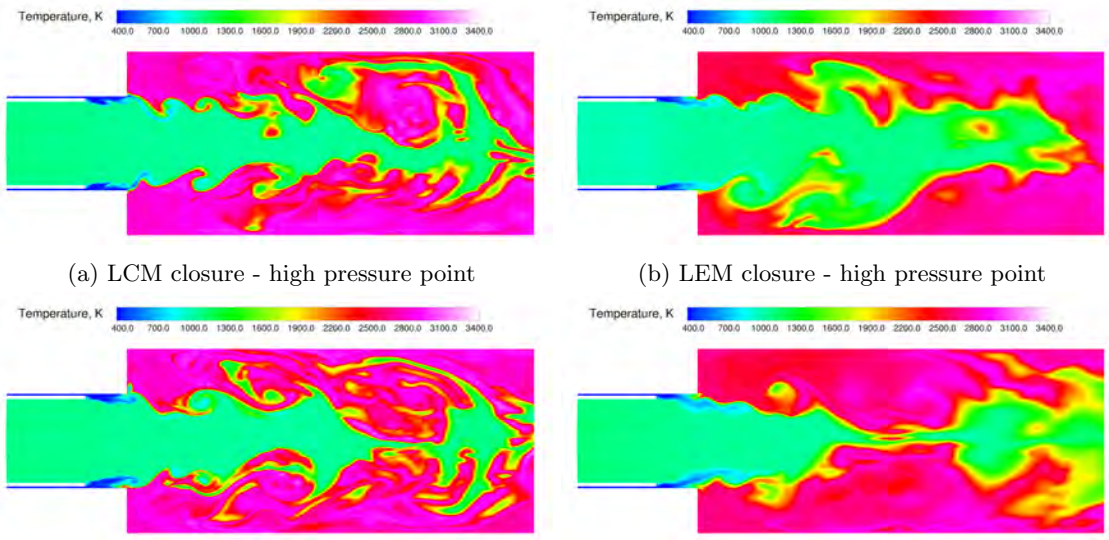

(a) LCM closure - high pressure point

(b) LEM closure - high pressure point

(c) LCM closure - low pressure point

(d) LEM closure - low pressure point

Figure 7: Temperature at the high and low pressure points of the cycle for the laminar and LEM solutions.

observed in the LEM results for this case.

The fuel mass fraction at the high pressure point of the cycle is shown in Figure 9. Notice how with the LCM closure there is a measurable amount of fuel present throughout the full 10 cm of the combustor shown. The methane is also concentrated in the shear layer region with little accumulation in the recirculation region. With the LEM closure the methane concentration is largely undetectable past 5 cm and there is a significant amount present in the recirculation region. This result confirms that very different burning mechanisms are operational in the two models.

Figure 10 takes a closer look at the different heat release dynamics using a much shorter time window. A series of five images spaced 0.02 ms apart depict the different dynamics that take place. For the LCM closure the vortex shed from the back step (signified by the circle) entrains the fuel and oxidizer. As it begins to mix, the heat release occurs primarily in the shear layer with some radial spreading into the core flow and towards the wall in snapshots four and five. For the LEM closure, the flow structure responsible for the burning is initially much larger and closer to the wall (also signified by the circle in the plot). The mixing between the fuel, oxidizer and recirculating gases takes place with very little burning. The burning that is taking place is concentrated in the near wall region where the stoichiometric mixture fraction and 2000 K isotherm cross (i.e., indicating a triple flame). As the process continues, the separation distance between the mixture fraction line and the 2000 K isotherm increases and burning takes place primarily near the wall. By snapshot four, there is intense heat release in two locations, near the wall and near the center of the chamber. By the final snapshot, we see a significant amount of heat release filling in the entire border of the flow structure. The rapid consumption of a large amount of fuel at a single time instance is clearly a feature of unstable combustion response and explains the higher instability amplitude observed in the LEM result.

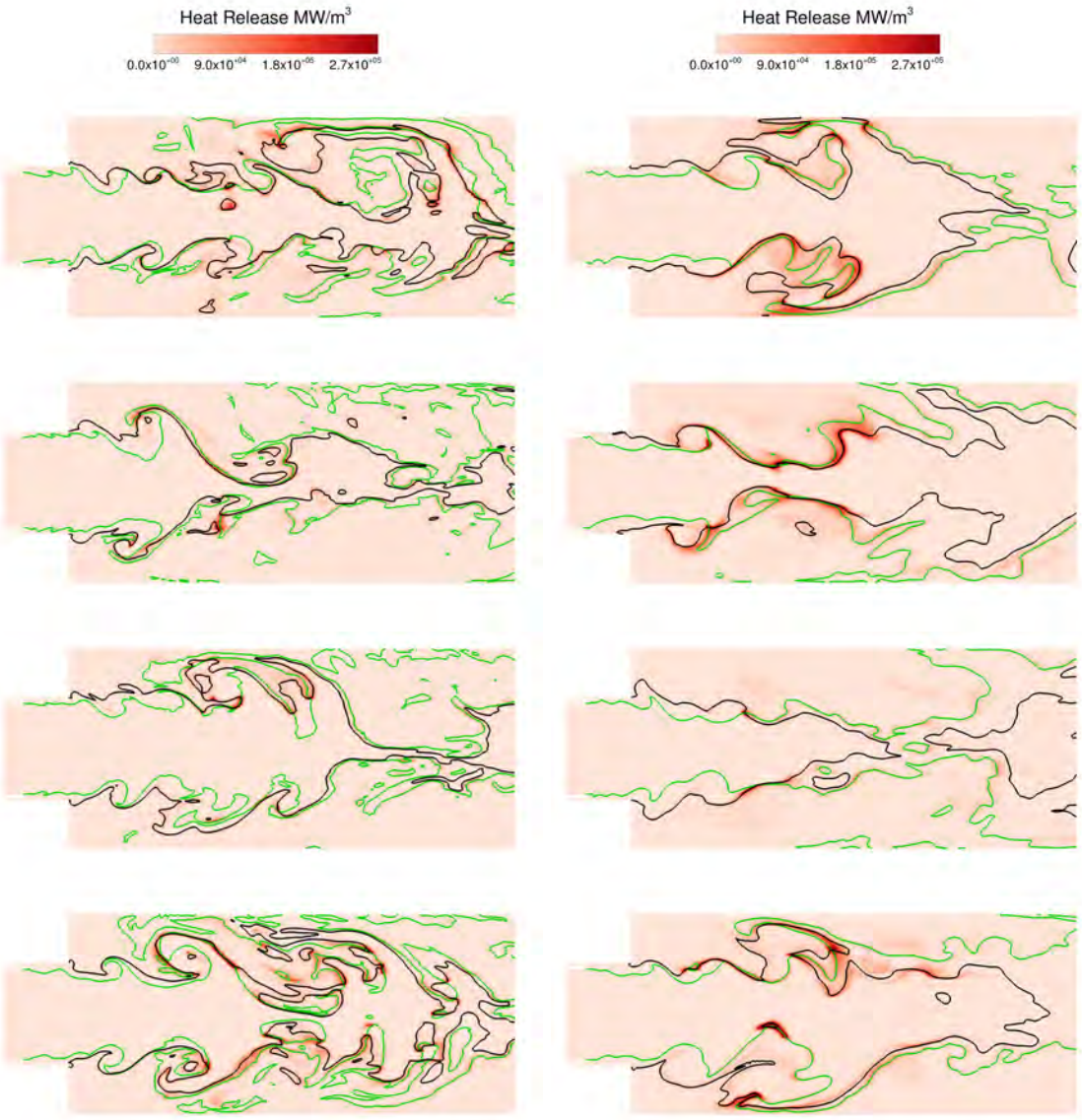

(a) LCM closure.

(b) LEM closure.

Figure 8: Heat release of the marginally stable operating point. The cycle begins with high pressure at the head end, the third snapshot is at the low pressure point and the final snapshot is during the rapid pressure rise. The contour is colored with heat release; the black line is a 2000 K isotherm which can be used to demarcate fresh and burnt gases. The green line is the stoichiometric mixture fraction.

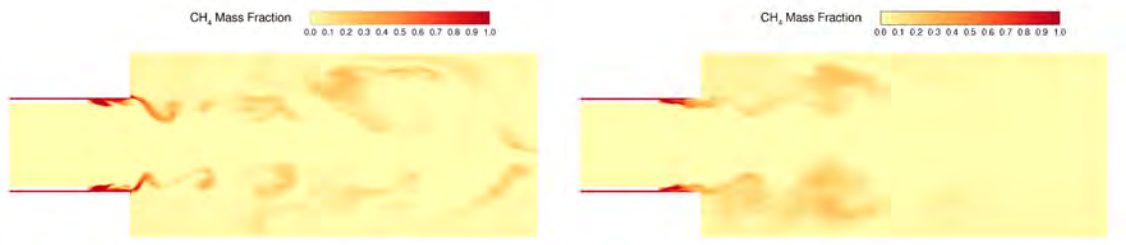

(a) LCM closure.

(b) LEM closure.

Figure 9: Fuel mass fraction contours at the head end of the combustor during the high pressure point of the cycle.

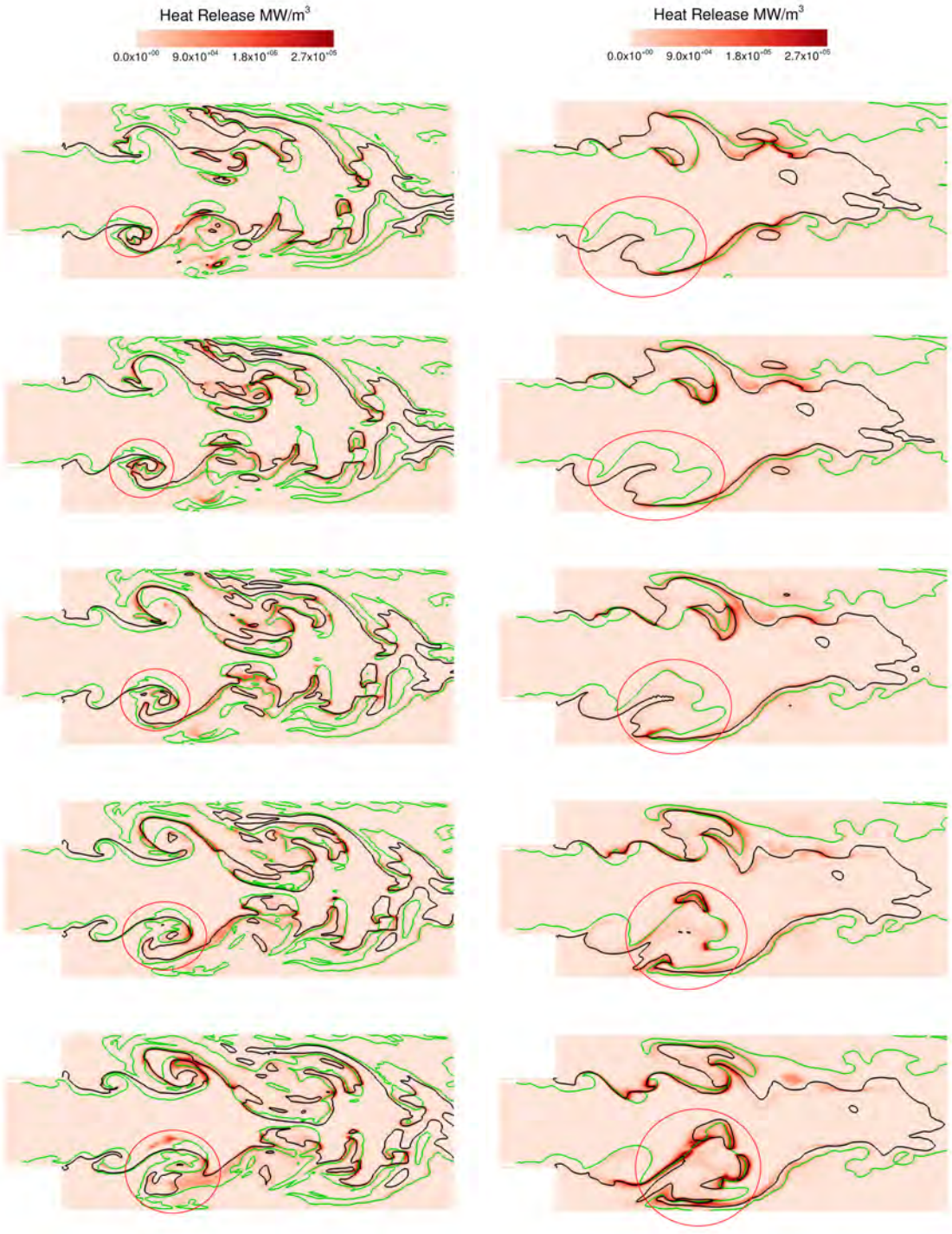

(a) LCM closure.

(b) LEM closure.

Figure 10: Heat release of the marginally stable operating point spaced 0.02 ms apart. The contour is colored with heat release; the black line is a 2000 K isotherm which can be used to demarcate fresh and burnt gases. The green line is the stoichiometric mixture fraction. Regions of interest are circled.

VI. Dynamics of the Unstable Operating Point

The differences between the predicted amplitude of the two closure models for the unstable operating point are not as large as for the marginally stable condition. Many of the differences in the flowfield observed in the marginally stable case are also present in the unstable case including the smoother flow features. However, in this case, both closure models predict qualitatively similar behavior and show concentrated heat release downstream of the dump plane that is in sync with the acoustic waves in the chamber. The dynamic heat release over a single acoustic cycle is shown in Figure 11. Again the cycle starts with the high pressure point

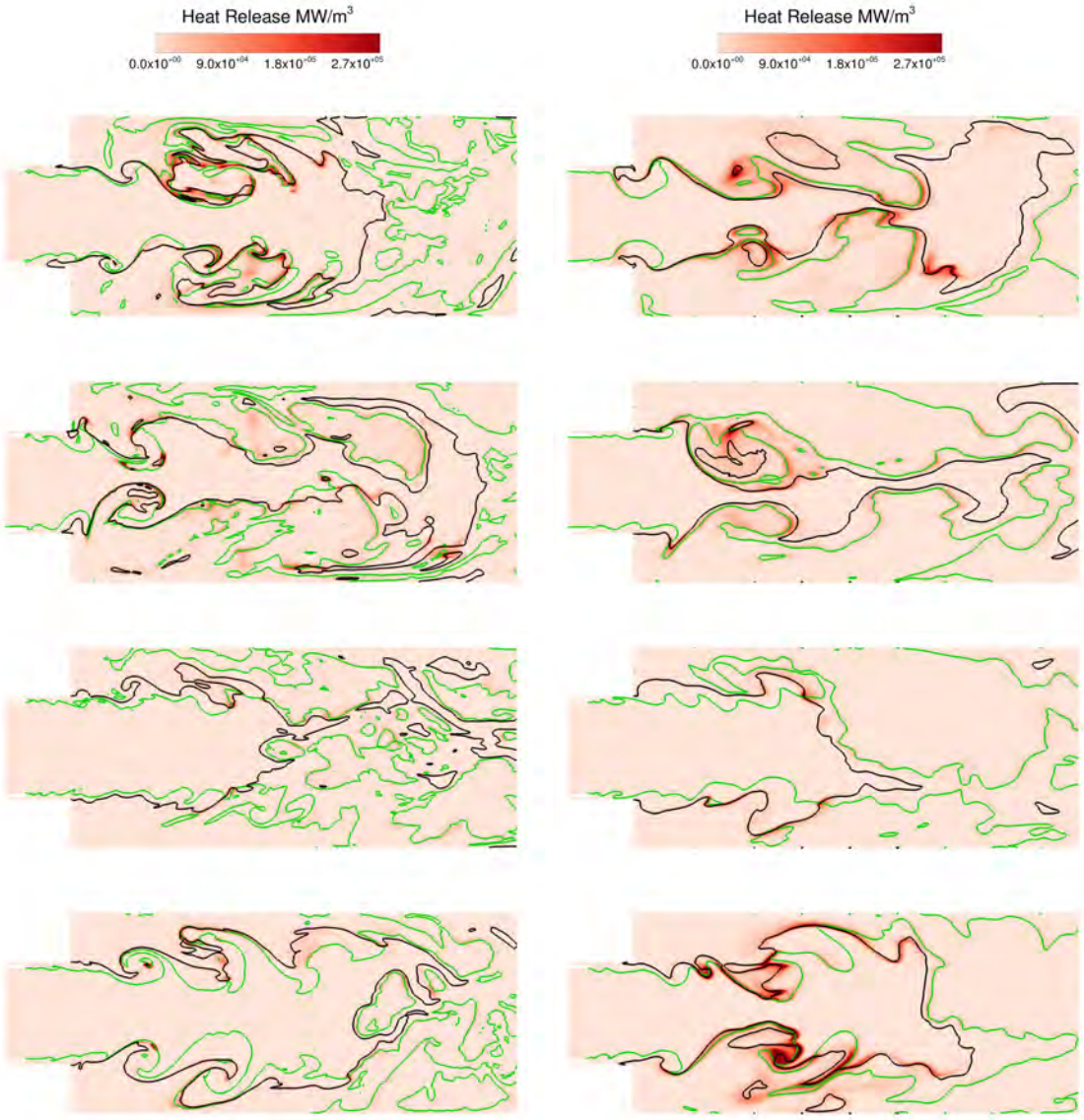

(a) LCM closure.

(b) LEM closure.

Figure 11: Heat release of the marginally unstable point. The cycle begins with high pressure at the head end, the third snapshot is at the low pressure point and the final snapshot is during the rapid pressure rise. The contour is colored with heat release; the black line is a 2000 K isotherm which can be used to demarcate fresh and burnt gases. The green line is the stoichiometric mixture fraction.

and both simulations show strong heat release occurring downstream from the dump plane. As the cycle progresses the heat release diminishes more quickly for the LCM closure and is distributed throughout the combustor while the LEM still predicts the majority of the combustion to be concentrated near the head

end with smaller amounts of lingering heat release taking place downstream. At the third snapshot both combustors are largely void of any heat release. The final snapshot shows more heat release taking place with the LEM closure indicating that the LEM reduces the recovery time of the fuel cut off event. This is likely the source for the lower amplitudes observed in the LEM results. Because the recovery time is shorter, less fuel is able to accumulate in the combustor leading to a smaller pressure spike when re-igniton occurs. In turn, this means that the LEM heat release is distributed over a longer period of the cycle, which reduces the degree of coupling between the chamber acoustics and the combustion.

The key aspects of the instability mechanism for the unstable oxidizer post length are the fuel cutoff event and the subsequent reignition event. The cutoff event is shown in Figure 12, which displays the fuel mass fraction and heat release contours for the LCM and LEM cases at the same time instance corresponding to the peak pressure at the combustor head-end. Both simulations show fuel displacement just inside the cup region. The effect is more pronounced in the laminar simulation. The fuel is replaced with warm products in the cup region adjacent to the wall near the dump plane. Both simulations show moderate heat release due to the combustion taking place in the cup region, which consumes the fuel before it enters the combustor. The heat release is largely coincident with the 2000 K isotherm. The fact that the fuel displacement is less severe in the LEM simulation also helps explain the shorter recovery time.

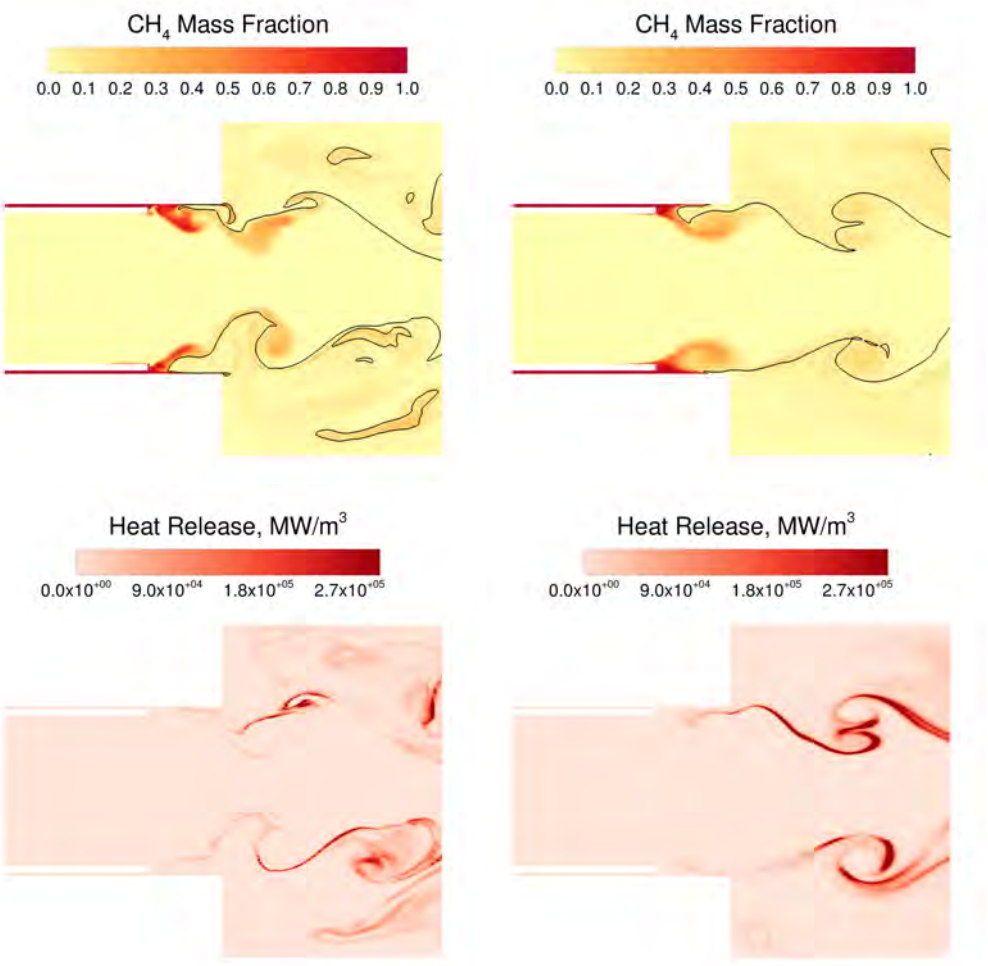

(a) LCM closure. (b) LEM closure.

Figure 12: Fuel cut off event. The top two images show the fuel mass fraction along with the 2000 K isotherm and the lower two figures show the combustion heat release at the same time instance.

The large reignition event that takes place is the result of the returning oxidizer post wave pushing the fuel into the warm recirculating gases. As seen in Figure 13 both simulations are able to capture the

interaction of the oxidizer pressure wave and the large amount of accumulated fuel at the head end of the combustor. The key difference is that some combustion has taken place downstream in the LEM simulation. Consequently, the fuel penetration distance in the combustor is not as great for the LEM. Again, this reduces the amplitude of the resulting post-ignition pressure spike because less fuel is available for the coupling event.

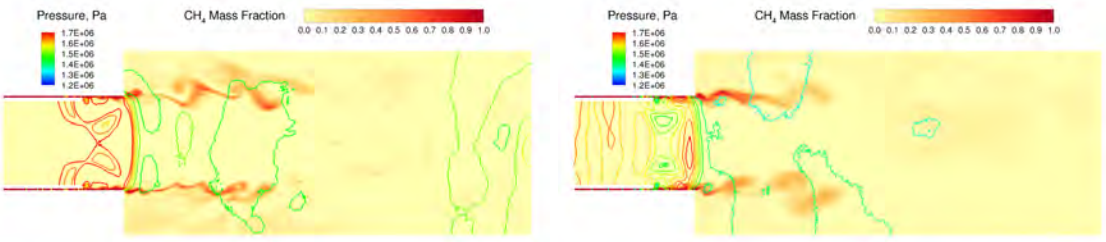

(a) LCM closure. (b) LEM closure.

Figure 13: Fuel reignition event from the oxidizer pressure pulse returning to the combustor. The background is colored with the fuel mass fraction and the lines are colored with static pressure. Both closures show the reignition event but the LEM simulation shows less fuel accumulated in the combustor.

VII. Summary

The linear eddy model has been applied to two combustion instability test cases and compared with companion simulations on identical meshes that used the laminar combustion model. The LEM is able to predict the marginally stable and unstable conditions correctly as is the LCM. The unstable LEM case becomes slightly more stable, while the marginally stable LEM case becomes somewhat more unstable than the LCM simulations. In both cases, our LEM results appear to be an improvement over previous reported LEM results[2] which showed a greater discrpancy between the simulation and experimental amplitudes. This is likely due to the finer grid used in the current study. However, the LEM trends are not uniformly better than the LCM results. Examination of the results of the two models indicates that there are significant differences in the flowfield for both operating conditions that can be correlated with the observed differences in the modal amplitudes. The LEM flowfield shows smoother flow features that are consistent with a thickened turbulent flame brush. The heat release is locally concentrated unlike in the LCM case, which shows a more distributed heat release pattern. For the unstable case, the combustion dynamics are quite similar: both simulations predict the fuel cutoff event, when the pressure wave crests at the combustor head-end, and the subsequent reignition event, that is timed with the return of the reflected pressure wave in the oxidizer post. The LEM simulation however begins to combust slightly ahead of the laminar simulation which reduces the effectiveness of the reignition event by consuming some of the available fuel, leading to slightly lower pressure amplitudes. The dynamics for the marginally stable case, however, shows a different heat release structure in the two models. In the LCM, the majority of the burning takes place in the shear layer, while for the LEM, the burning occurs in a large flow structure, which interacts with the wall and recirculating gases. This structure traps the fuel and causes more fuel to burn at once, leading to higher coupling with the chamber acoustics and, consequently, higher pressure amplitudes. Overall, the present LEM results are not a significant improvement over the LCM results. Some of the discrepancies may well be related to the limitations of the LEM model for finer grids, wherein the errors due to the lack of large-scale species diffusion and the arbitrariness of the Lagrangian splicing may introduce errors. Further study including systematic grid resolution is necessary to elucidate these performance trends.

Acknowledgments

Computing resources were provided by the DoD High Performance Computing Modernization Program.

References

[1]Harvazinski, M., Huang, C., Sankaran, V., Feldman, T., Anderson, W., Merkle, C., and Talley, D., "Coupling between hydrodynamics, acoustics, and heat release in a self-excited unstable combustor," *Physics of Fluids*, Vol. 27, 2015, pp. 045102.

[2]Srinivasan, S., Ranjan, R., and Menon, S., "Flame Dynamics During Combustion Instability in a High-Pressure, Shear-Coaxial Injector Combustor," *Flow Turbulence and Combustion*, Vol. 94, No. 1, 2015, pp. 237–262.

[3]Garby, R., Selle, L., and Poinsot, T., "Large-Eddy Simulation of Combustion Instabilities in a Variable-length Combustor," *Comptes Rendus Mécanique*, Vol. 341, No. 1-2, 2013, pp. 220–229.

[4]Pitsch, H. and Peters, N., "A Consistent Flamelet Formulation for Non-Premixed Combustion Considering Differential Diffusion Effects," *Combustion and Flame*, Vol. 1-2, 1998, pp. 26–40.

[5]Givi, P., "Filtered Density Functions for Subgrid Scale Modeling of Turbulent Combustion," *AIAA Journal*, Vol. 44, 2006, pp. 16–23.

[6]Pope, S., "Small scales, many species and the manifold challenges of turbulent combustion," *Proceedings of the Combustion Institute*, Vol. 34, 2013, pp. 1–31.

[7]Kerstein, A., "Linear-eddy modeling of turbulent transport," *Combustion and Flame*, Vol. 75, 1989, pp. 397–413.

[8]Colin, O., Ducros, F., Veynante, D., and Poinsot, T., "A Thickened Flame Model for Large Eddy Simulations of Turbulent Premixed Combustion," *Physics of Fluids*, Vol. 12, No. 7, 2000, pp. 1843–1863.

[9]Sankaran, V. and Merkle, C., "Fundamental Physics and Model Assumptions in Turbulent Combustion Models for Aerospace Propulsion," *50th AIAA/ASME/SAE/ASEE Joint Propulsion Conference and Exhibit*, AIAA, Cleveland, OH, July 2013, pp. 1–14.

[10]Yu, Y., Sisco, J., Rosen, S., Madhav, A., and Anderson, W., "Spontaneous Longitudinal Combustion Instability in a Continuously-Variable Resonance Combustor," *Journal of Propulsion and Power*, Vol. 28, No. 5, 2012, pp. 876–887.

[11]Menon, S. and Kerstein, A., "Stochastic simulation of the structure and propagation rate of turbulent premixed flames," *Proceedings of the combustion institute*, Vol. 24, 1992, pp. 443–450.

[12]Menon, S. and Kerstein, A., "The linear-eddy model," *Turbulent Combustion Modeling of Fluid Mechanics and its Applications*, edited by T. Echekki and E. Mastorakos, Springer, New York, 2011, pp. 221–247.

[13]Harvazinski, M., Huang, C., Sankaran, V., Feldman, T., Anderson, W., Merkle, C., and Talley, D., "Instability Mechanism in a Pressure-coupled Gas-gas coaxial rocket injector," *49th AIAA/ASME/SAE/ASEE Joint Propulsion Conference and Exhibit*, AIAA, San Jose, CA, July 2013, pp. 1–21.

[14]Kim, W., Menon, S., and Mongia, H., "Large Eddy Simulation of Gas Turbine Combustor Flow," *Combustion Science and Technology*, Vol. 143, 1999, pp. 25–62.

[15]Génin, F. and Menon, S., "Simulation of Turbulent Mixing Behind a Strut Injector in Supersonic Flow," *AIAA Journal*, Vol. 48, 2010, pp. 526–539.

[16]Génin, F. and Menon, S., "Studies of shock/turbulent Shear Layer Interaction Using Large-eddy Simulation," *Computers and Fluids*, Vol. 39, 2010, pp. 800–819.

[17]Masquelet, M. and Menon, S., "Large Eddy Simulation of Flame-Turbulence Interactions in a Shear Coaxial Injector," *Journal of Propulsion and Power*, Vol. 26, 2010, pp. 924–935.

[18]Franzelli, B., Riber, E., Gicquel, L., and Poinsot, T., "Large Eddy Simulation of combustion instabilities in a lean partially premixed swirled flame," *Combustion and Flame*, Vol. 159, 2012, pp. 621–637.

[19]Feldman, T., Harvazinski, M., Merkle, C., and Anderson, W., "Comparison Between Simulation and Measurement of Self-Excited Combustion Instability," *48th AIAA/ASME/SAE/ASEE Joint Propulsion Conference and Exhibit*, AIAA, Atlanta, GA, July 2012, pp. 1–8.

[20]Garby, R., Selle, L., and Poinsot, T., "Analysis of the impact of heat losses on an unstable model rocket-engine combustor using large-eddy simulation," AIAA, Atlanta, GA, July 2012, AIAA Paper 2012-4085.

Comparison of Laminar and Linear Eddy Model Closures for Combustion Instability Simulations

Matt Harvazinski, Doug Tally, & Venke Sankaran
Air Force Research Laboratory
Edwards AFB, CA

Outline

- **Introduction**
- **Turbulent combustion and the linear eddy model**
- **Simulation results**
  - Marginally stable operating condition
  - Unstable operating condition
- **Summary**

History

Combustion instability is an organized, oscillatory motion in a combustion chamber sustained by combustion.

CI caused a four year delay in the development of the F-1 engine used in the Apollo program

> 2000 full scale tests

> $400 million for propellants alone (2010 prices)

Irreparable damage can occur in less than 1 second.

Damaged engine injector faceplate caused by combustion instability

"Combustion instabilities have been observed in almost every engine development effort, including even the most recent development programs"

– JANNAF Stability Panel Draft (2010)

Challenges

The laminar combustion model (LCM) assumes:

$$\widetilde{\dot{\omega}} = \dot{\omega}\left(\widetilde{T}, \widetilde{Y_k}\right)$$

When in reality it should be:

$$\widetilde{\dot{\omega}} = \int_{T_{\min}}^{T_{\max}} \int_0^1 \dot{\omega}\left(Y_k, T\right) \widetilde{P}\left(Y_k, T; \mathbf{x}, t\right) \mathrm{d}Y_k \, \mathrm{d}T$$

Compute directly from finite rate kinetics

Joint-PDF, how do we compute it?

Turbulent Combustion Models

Model	Key Assumptions	Solution Process	Validity
Flamelets (Non-premixed) G-Equation (premixed)	• 1D, Steady, laminar velocity field • Equal diffusion coefficients • Presumed-PDF • Low Mach	• Solves Z, Z" eqns • Reaction progress variable • Tabulated reactive scalars • Derived filtered quantities	• Low Mach • High Da • Low Re
Linear Eddy Model Premixed/Non-premixed	• Sub-grid transport • 1D const pressure in sub-grid * Exact combustion	• Species convection in LES grid • 1D reaction-diffusion in LEM grid	• All regimes (low-Mach?)
PDF-Transport Premixed/Non-premixed	• Scalar-mixing transport assumptions • Treats combustion source exactly	• Solves for PDF-transport using Langevin eqn and Langragian method	• Low Mach • All Da • All Re

Sankaran, V. and Merkle, C. Fundamental Physics and Model Assumptions In Turbulent Combustion Models for Aerospace Propulsion, AIAA 2014-3941, 50th AIAA/ASME/SAE/ASEE Joint Propulsion Conference, July 2014.

Linear Eddy Model

Construct 1-D LEM cells in each LES cell, the resolution of the 1-D cell should be commensurate with the Kolmogorov length scale

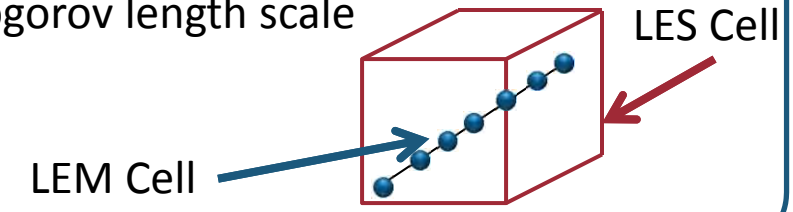

Solve 1-D conservation equations for species and energy:

$$\frac{\partial Y_k}{\partial t} = F_{k,\text{stir}} - \frac{1}{\rho}\frac{\partial}{\partial s}\left(\rho Y_k V_k\right) + \frac{\dot{\omega}_k}{\rho}$$

$$\frac{\partial T}{\partial t} = F_{T,\text{stir}} - \frac{1}{c_p}\sum_{k=1}^{N} c_{p,k} Y_k V_k \frac{\partial T}{\partial s} + \frac{1}{\rho c_p}\frac{\partial}{\partial s}\left(\lambda \frac{\partial T}{\partial s}\right) + \frac{1}{\rho c_p}\sum_{k=1}^{N} \Delta h^{\circ}_{f,k}\dot{\omega}_k$$

Linear Eddy Model

The stirring term introduces a “1D” eddy into the profile, the size and frequency of the stirring is controlled by stochastic equations

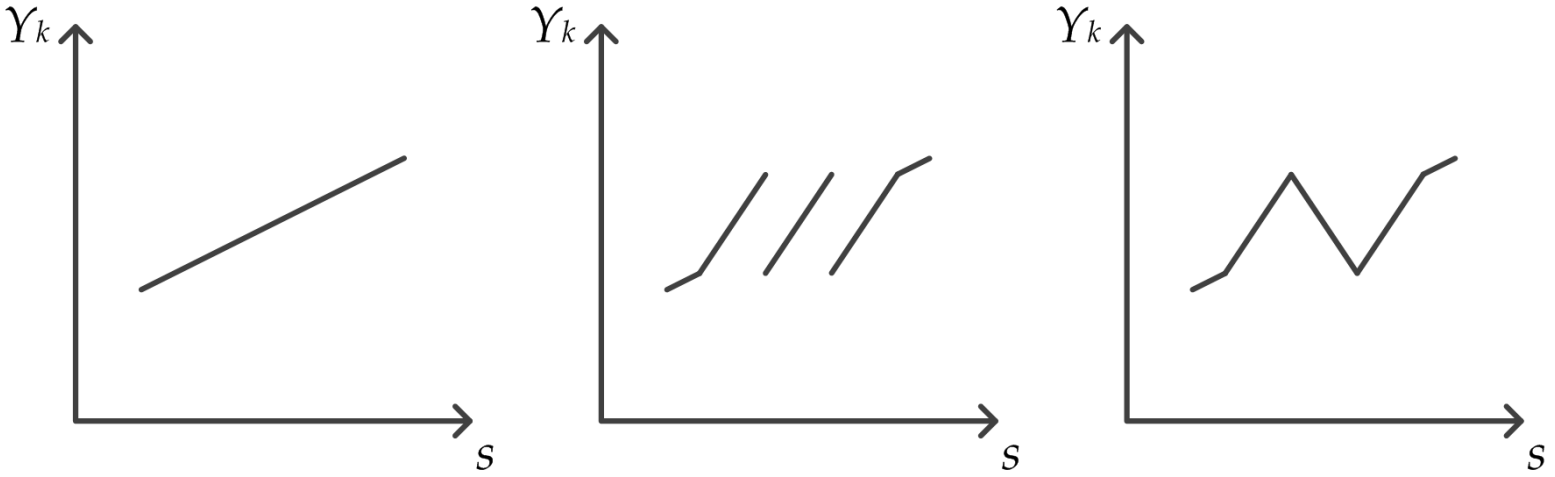

Original Profile

Length is reduced by a factor of 3 and copied twice

Center segment is mirrored to conserve mass

Linear Eddy Model

Not strictly a sub-grid model. Lagrangian splicing model, no resolved scale Eulerian transport of species.

No resolved scale diffusion -> not DNS consistent

Mass is transferred is "random"

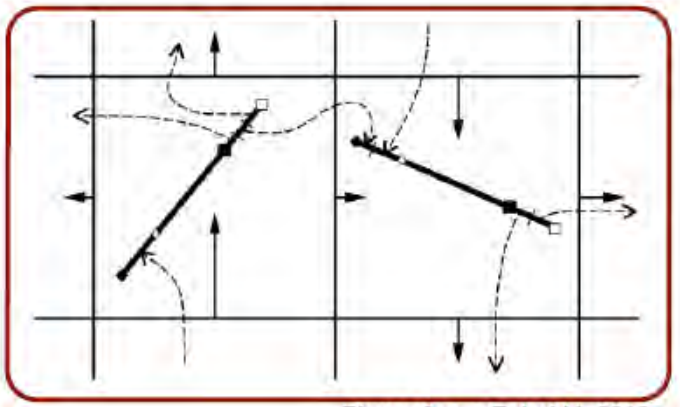

Figure from: Echekki, 2010.

Two temperatures, a resolved scale and sub-grid temperate. How well coupled is the energy transfer between the large scale and sub-grid?

Longitudinal Experiment

Continuously Varying Resonance Chamber

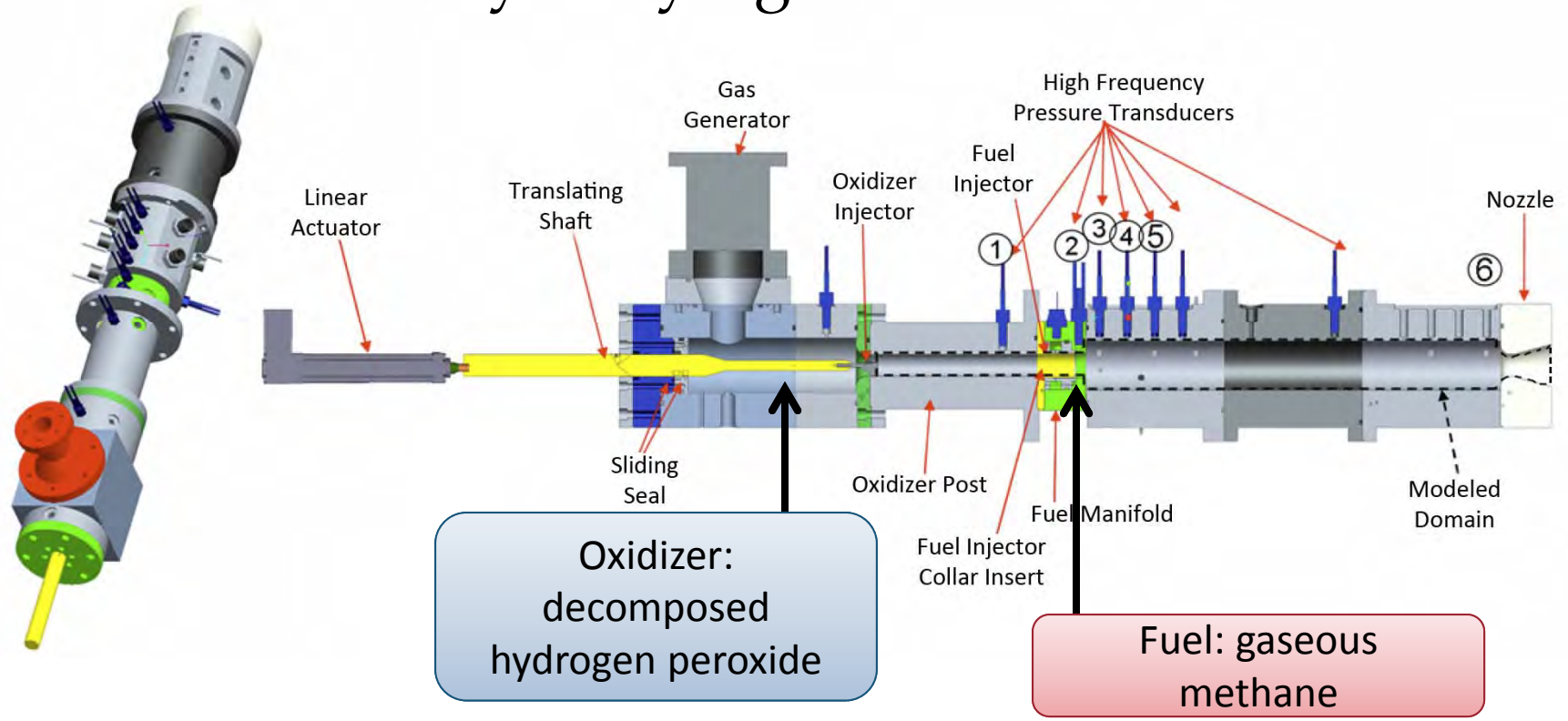

Yu et al. 2013

Experimental Results

Unsteady pressure for a translating test

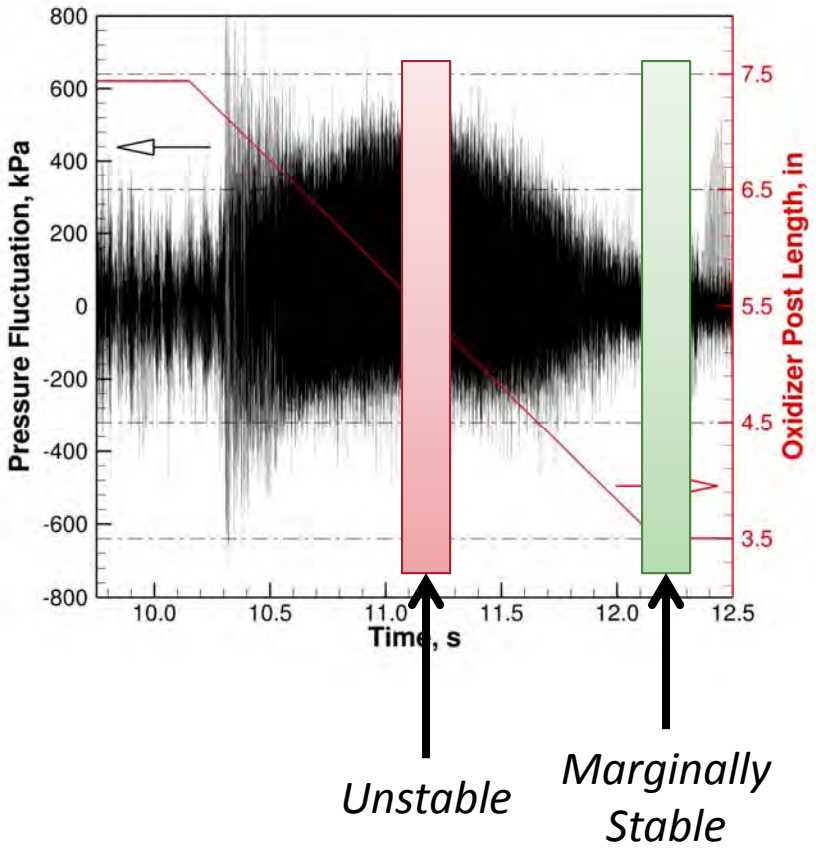

PSD power for the first mode

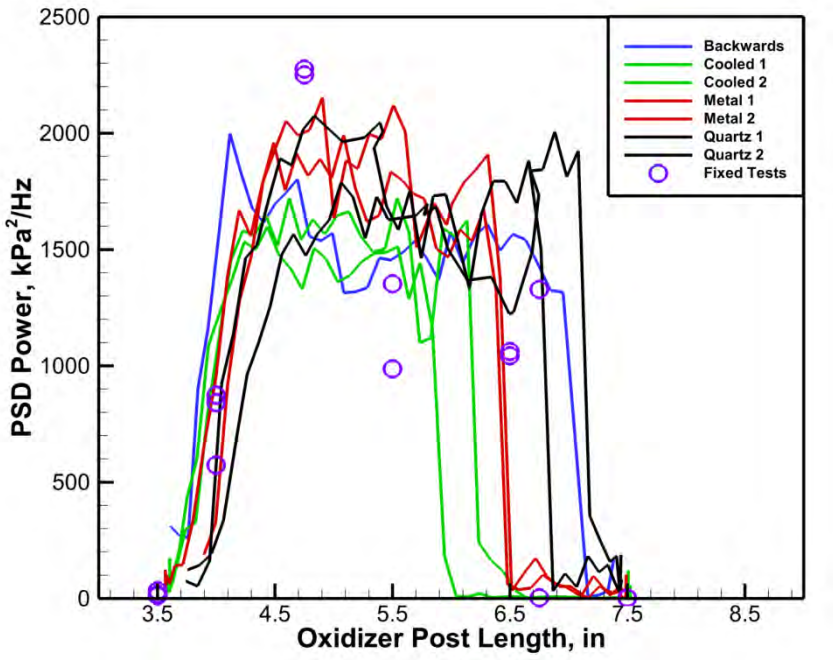

Harvazinski et al. 2013

Instability Mechanism

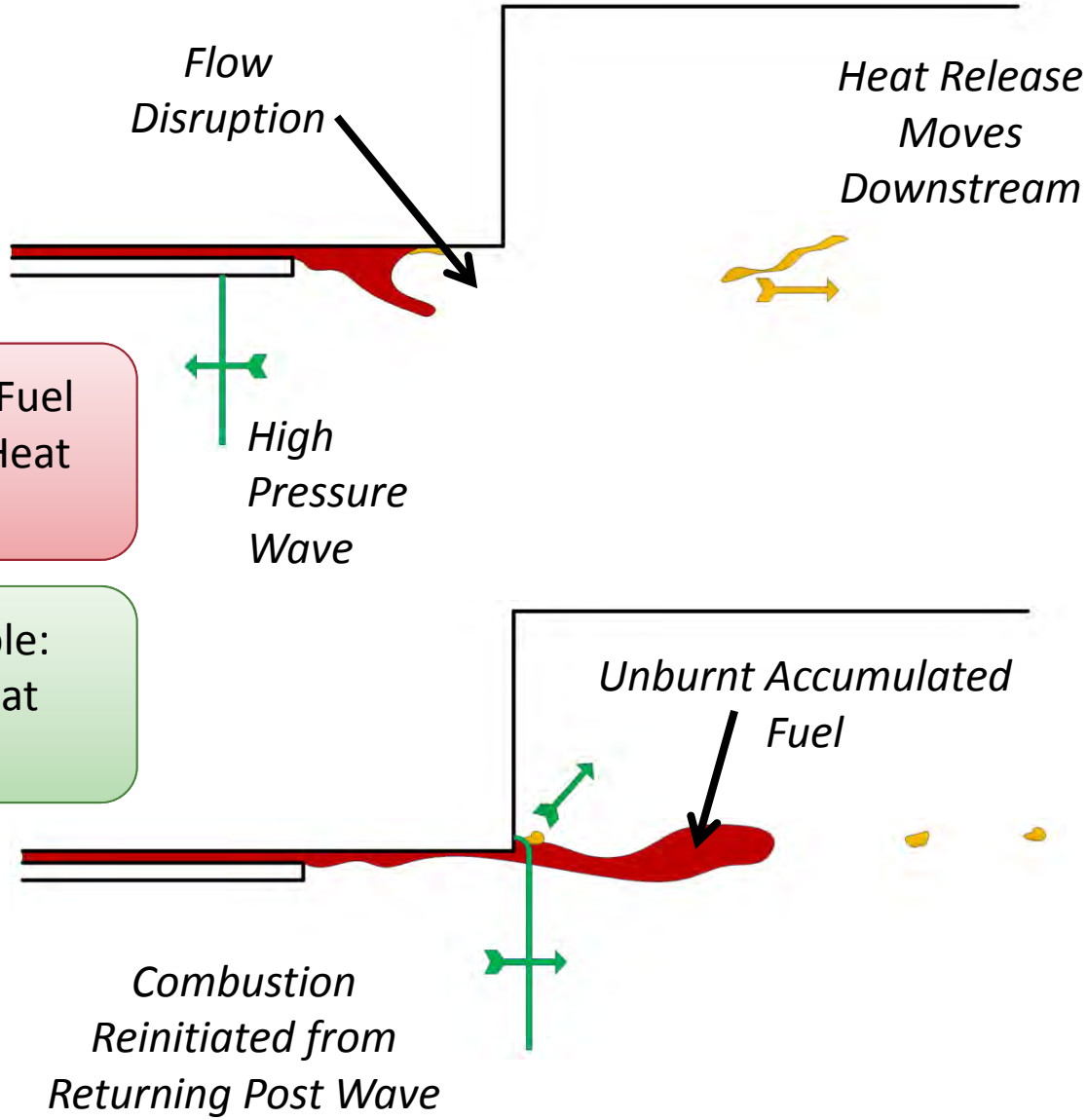

Unstable: Cyclic Fuel Disruption and Heat Release

Marginally Stable: Continuous Heat Release

Simulation Details

- Solver: LESLIE3D
- hybrid second-order central and third-order MUSCL scheme
- Explicit McCormack's method
- Unsteady reacting flow LES
- LCM and LEM available
- Adiabatic walls, constant mass flow inlets

- Two oxidizer post lengths were simulated:
  - 8.89 cm
  - 13.97 cm
- Mesh size:
  - 8.6 M
  - 8.9 M
  - Identical except for the oxidizer post length

Operating Conditions

Parameter	Value
Oxidizer Composition	57.6% H_2O, 42.4% O_2
Oxidizer temperature, K	1030
Oxidizer flow rate, kg/s	0.320
Fuel Composition	100% CH_4
Fuel temperature, K	300
Fuel flow rate, kg/s	0.027
Nozzle back pressure, kPa	101.325

Two-step global model

$$CH_4 + \frac{3}{2}O_2 \longrightarrow CO + 2\,H_2O$$

$$CO + \frac{1}{2}O_2 \longrightarrow CO_2$$

Pressure Time History

Marginally Stable

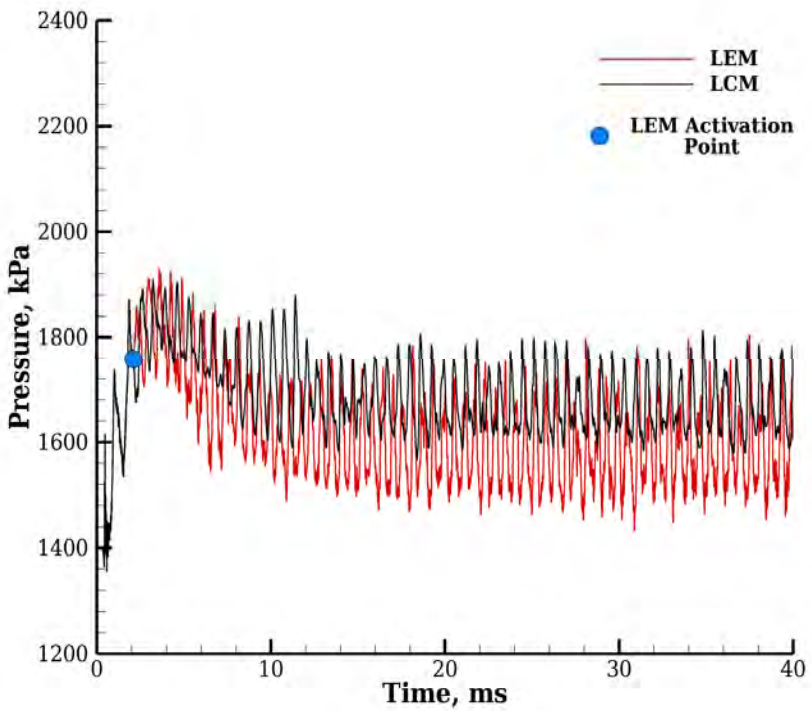

Unstable

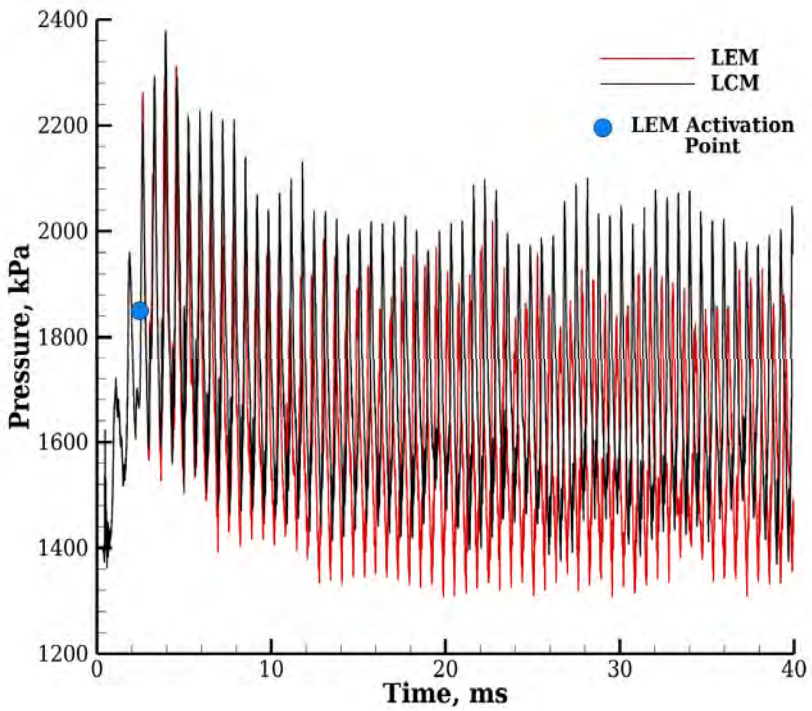

Fluctuating Pressure

Marginally Stable

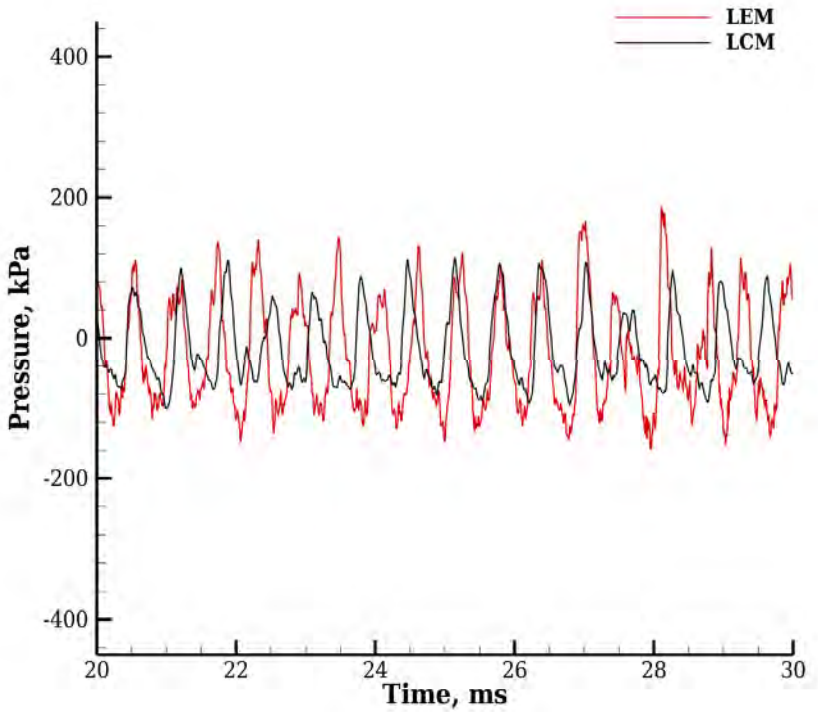

Unstable

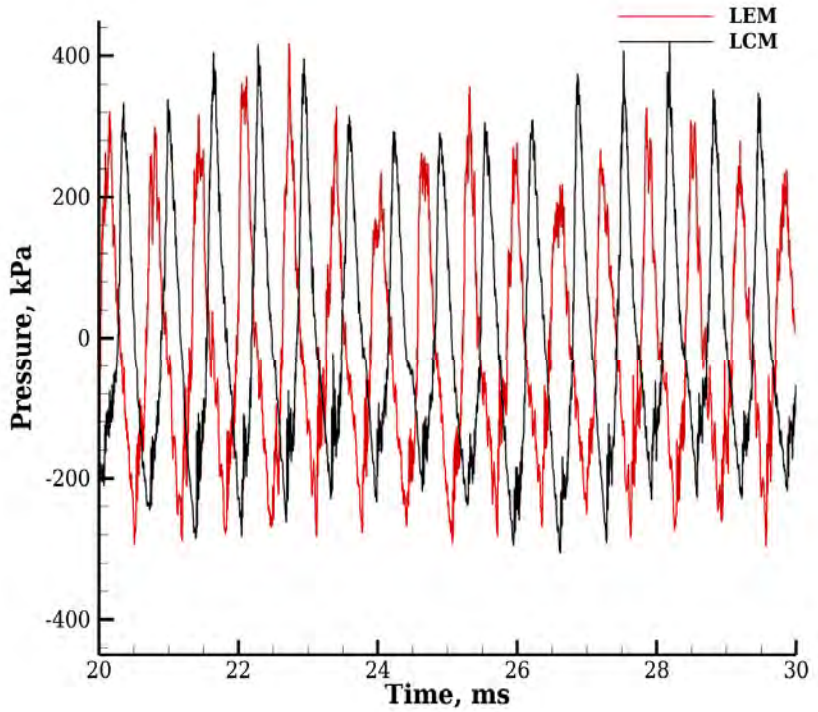

PSD Marginally Stable

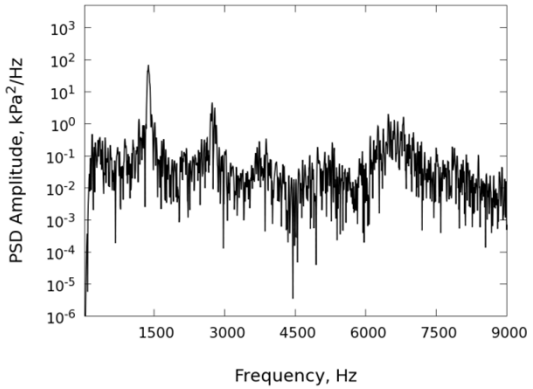

- LCM shows good agreement with the experiment (left), while LEM has a higher amplitude
- Both show distensible first and second modes like the experiment but overpredict the second mode amplitude

LCM

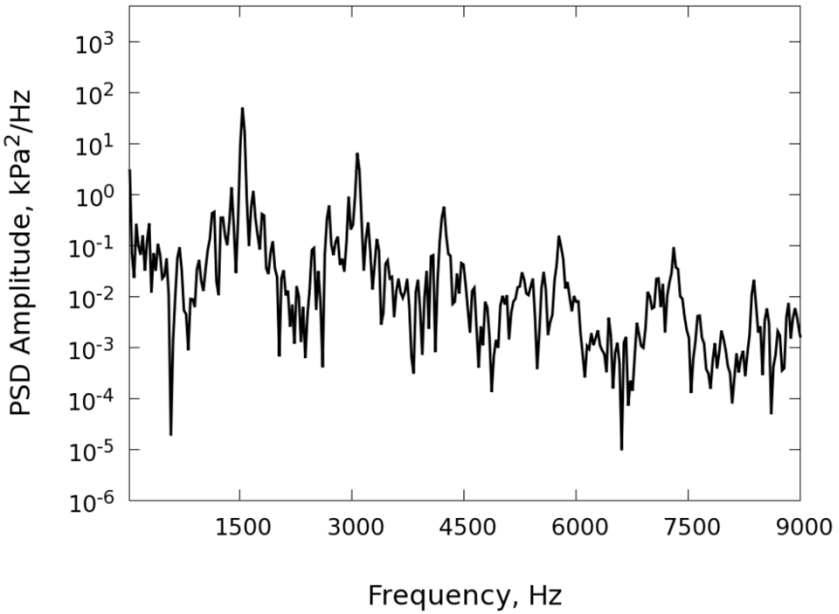

LEM

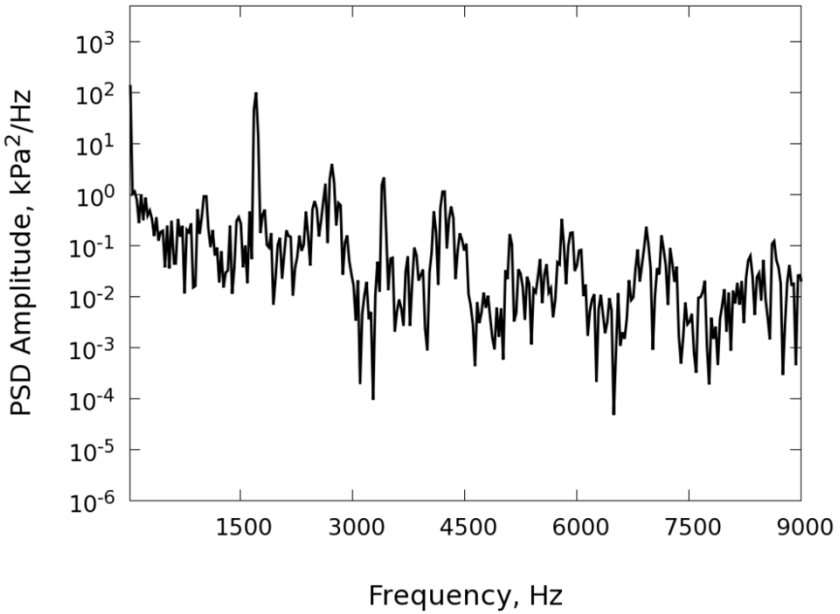

PSD Marginally Stable

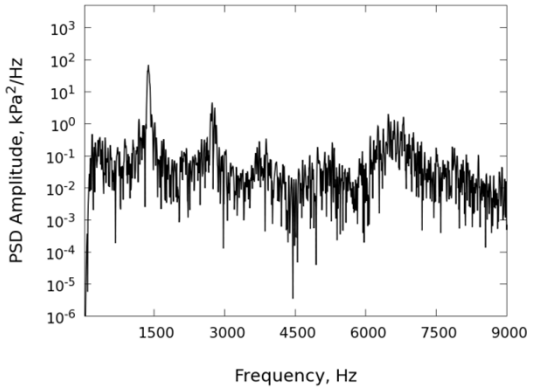

- LCM shows good agreement with the experiment (left), while LEM has a higher amplitude
- Both show distensible first and second modes like the experiment but overpredict the second mode amplitude

Mode	Experiment			LCM			LEM		
	f, Hz	p'_{ptp}, kPa	f_i/f_1	f, Hz	p'_{ptp}, kPa	f_i/f_1	f, Hz	p'_{ptp}, kPa	f_i/f_1
1	1379	121.70	1.00	1536	95.50	1.00	1710	146.63	1.00
2	2734	5.86	1.98	3072	36.89	2.00	2725	34.00	1.59
3	3882	16.03	2.82	4232	12.71	2.76	4203	21.12	2.46
Total		143.06			145.10			201.75	

PSD Unstable

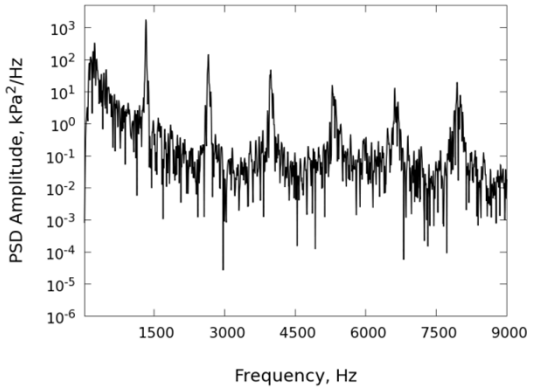

- Both LCM and LEM have a lower amplitude compared to the experiment
- LEM modes 4 & 5 show a bifurcation not seen in the experiment

LCM

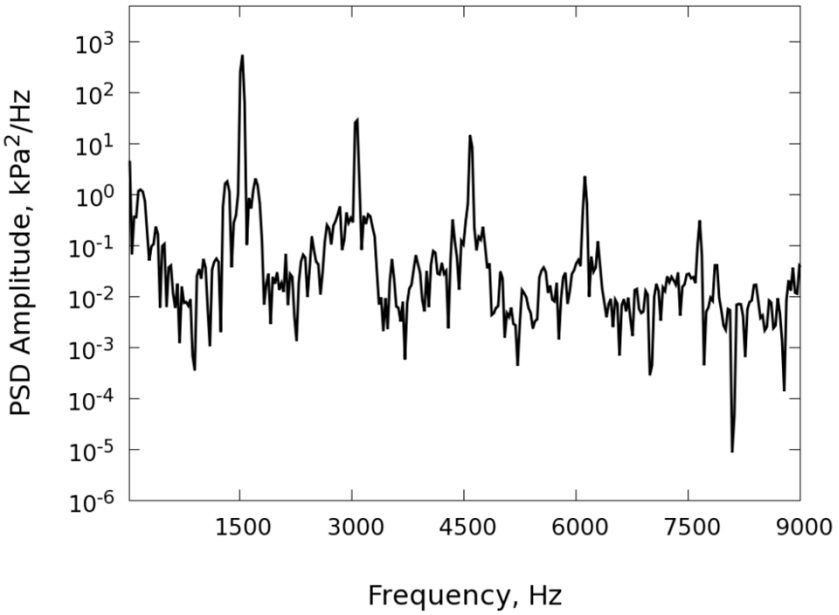

LEM

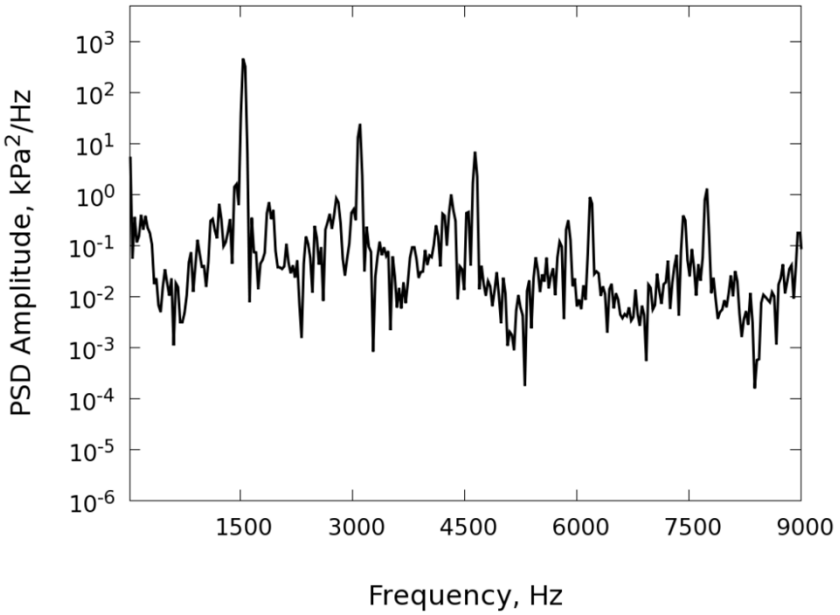

PSD Unstable

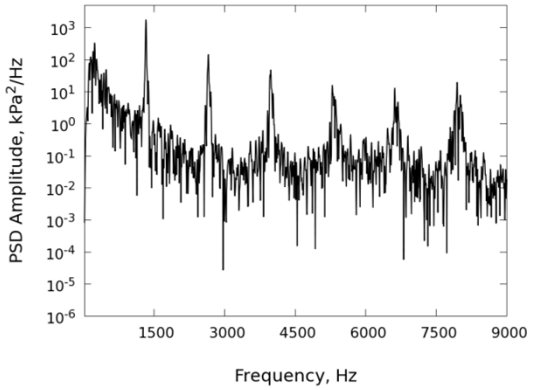

- Both LCM and LEM have a lower amplitude compared to the experiment
- Both LCM and LEM predict harmonic nature of the higher modes

Mode	Experiment			LCM			LEM		
	f, Hz	p'_{ptp}, kPa	f_i/f_1	f, Hz	p'_{ptp}, kPa	f_i/f_1	f, Hz	p'_{ptp}, kPa	f_i/f_1
1	1324	387.15	1.00	1536	337.42	1.00	1536	333.22	1.00
2	2655	89.29	2.01	3073	89.27	2.00	3101	69.78	2.02
3	3979	46.37	3.01	4580	54.77	2.98	4638	36.15	3.02
4	5296	41.97	4.00	6116	19.62	3.98	6174	14.90	4.02
Total		564.78			501.08			454.05	

Comparison to other Work

Prior Work

	Harvazinski et al.[1]	Srinivasan et al.[2]	Garby et al.[3]
Code	GEMS	LESLIE3D	AVBP
Turbulence Model	DES	LES	LES
Combustion Closure	Laminar	LEM	DTF
Grid Size	5 M	1.4 M	14 M
Post Lengths, cm	8.89, 13.97, 19.05	9.0, 12.0, 14.0	12.0
$f_1/f_{1,\text{exp}}$	1.24, 1.16, 1.18	1.2, 1.16, 1.19	1.09
$A_1/A_{1,\text{exp}}$	1.07, 0.90, 1.93	4.34, 0.34, 0.47	Not Reported

Better amplitude predictions than prior LEM work.
Possible due to a finer grid.

Frequency predicitons are on par with other studies.

Current Work

Case	$f_1/f_{1,\text{exp}}$	$A_1/A_{1,\text{exp}}$
Marginally Stable, LCM	1.11	0.780
Marginally Stable, LEM	1.24	1.20
Unstable, LCM	1.16	0.872
Unstable, LEM	1.16	0.861

Marginally Stable Flowfield

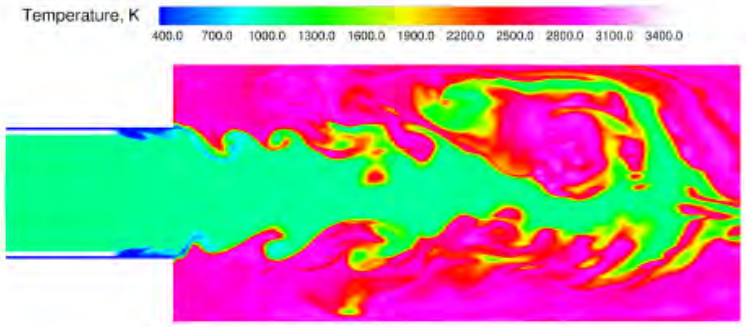

(a) LCM closure - high pressure point

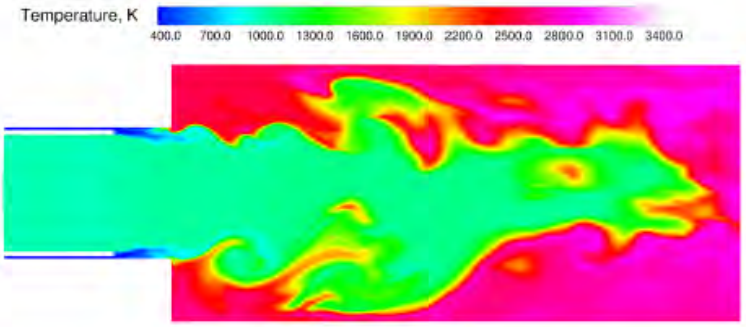

(b) LEM closure - high pressure point

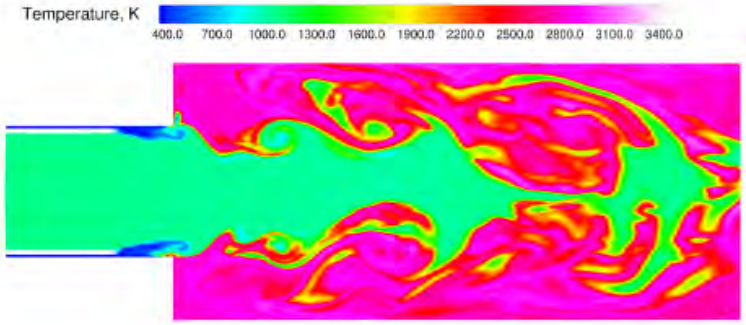

(c) LCM closure - low pressure point

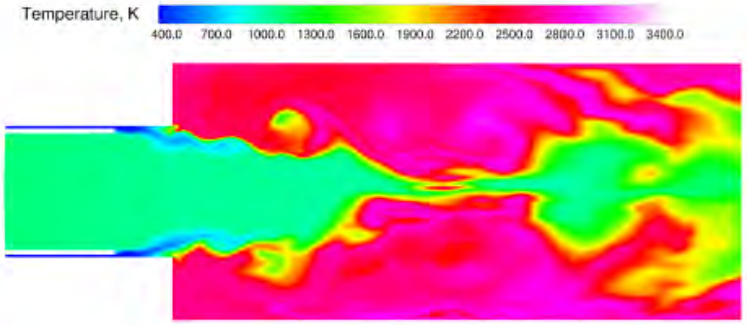

(d) LEM closure - low pressure point

- LEM has less resolved flow features
- Acoustic length scales are large compared to these features

Heat Release Cycle

LCM

LEM

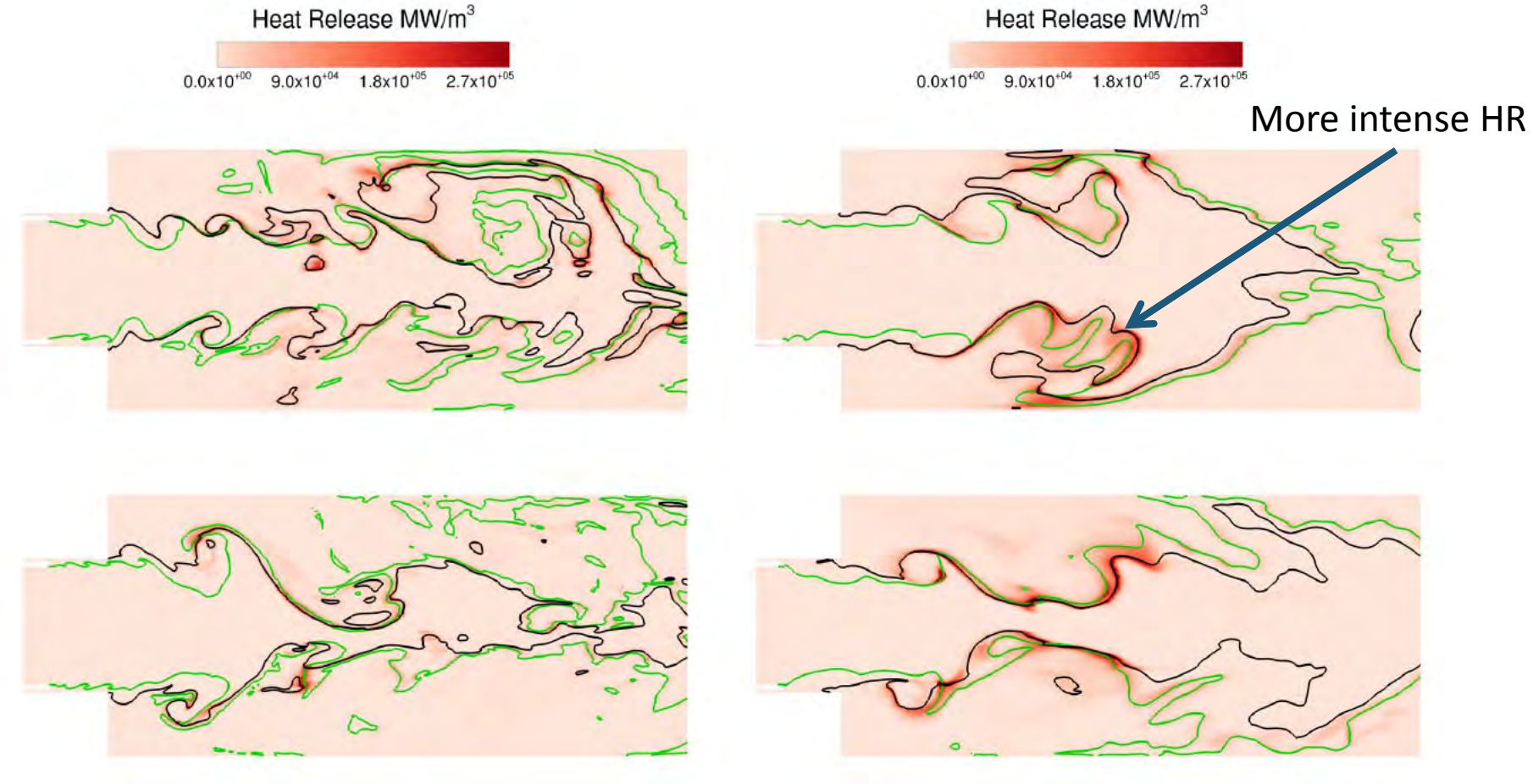

Heat Release Cycle

LCM

LEM

Both show a decease in the amount of HR at the low point of the cycle

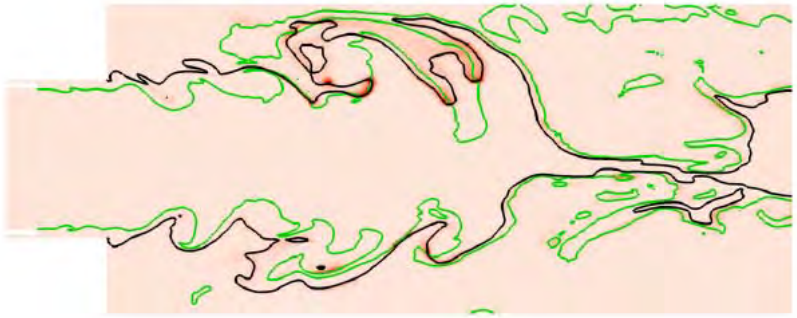

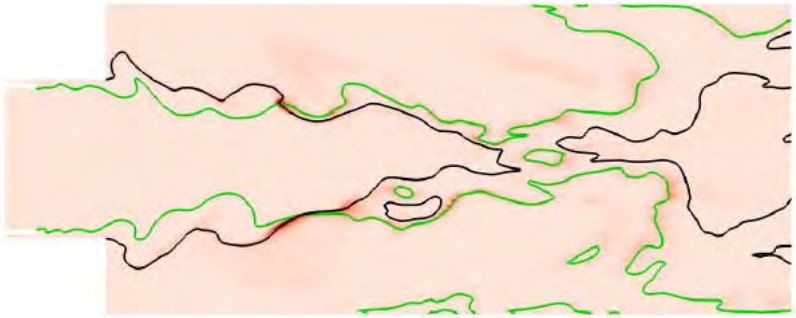

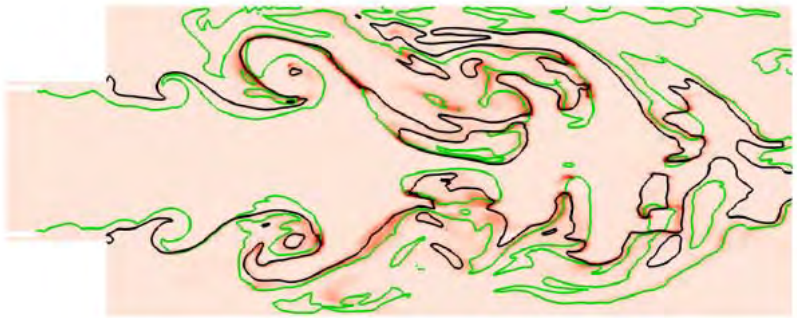

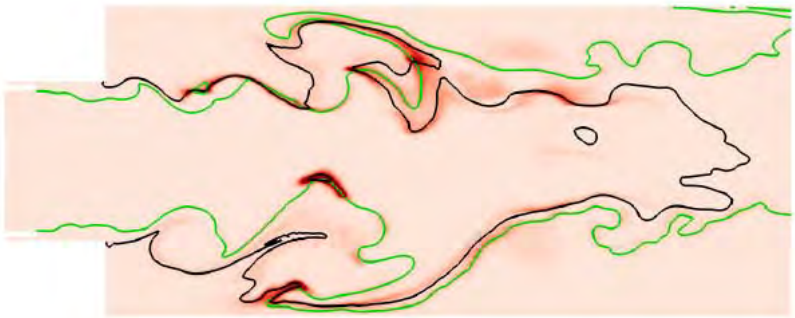

Heat release is more distributed

Heat release is more concentrated and intense

Fuel Mass Fraction

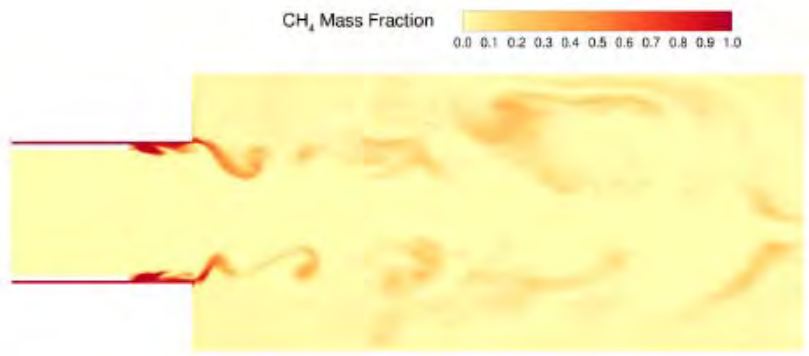

(a) LCM closure.

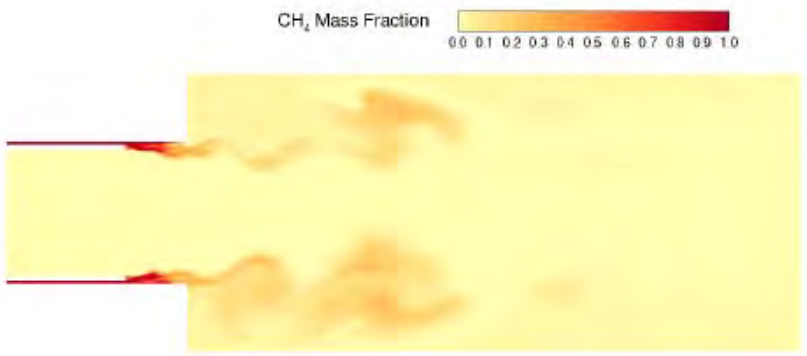

(b) LEM closure.

More complete combustion in the case of LEM. Almost no measurable fuel downstream. This may be the source of the higher amplitudes.

Heat Release – Take 2

LCM

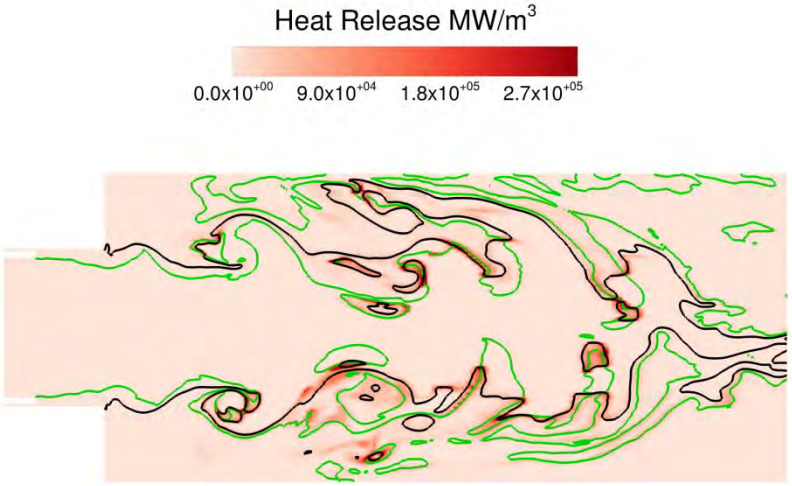

LEM

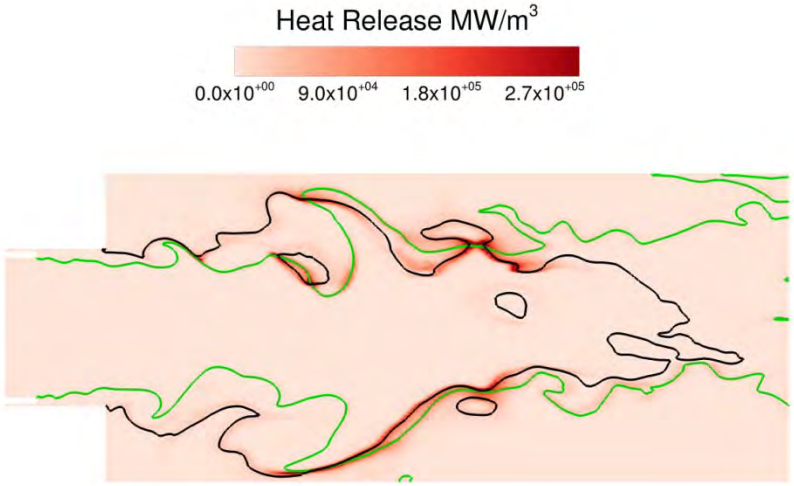

Heat Release – Take 2

LCM

LEM

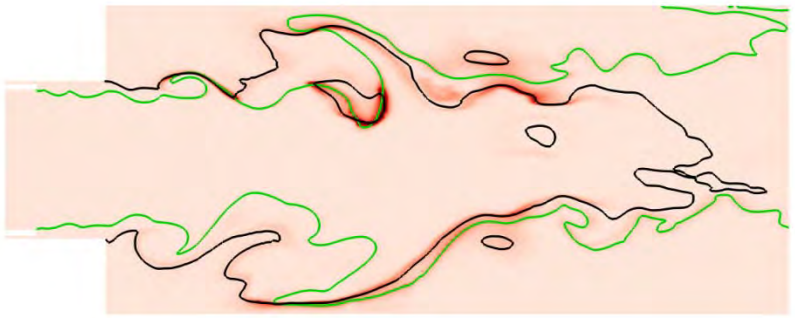

Heat Release – Take 2

LCM

LEM

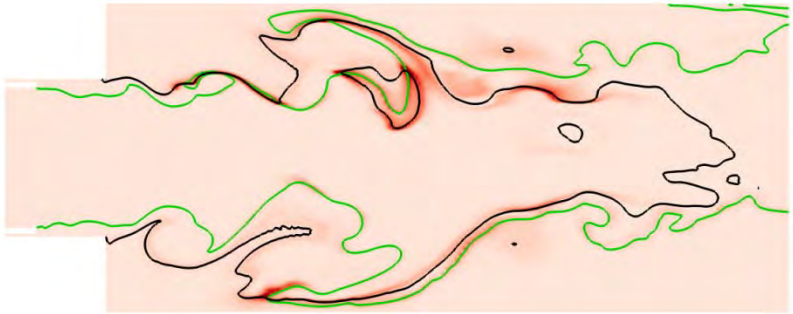

Heat Release – Take 2

LCM

LEM

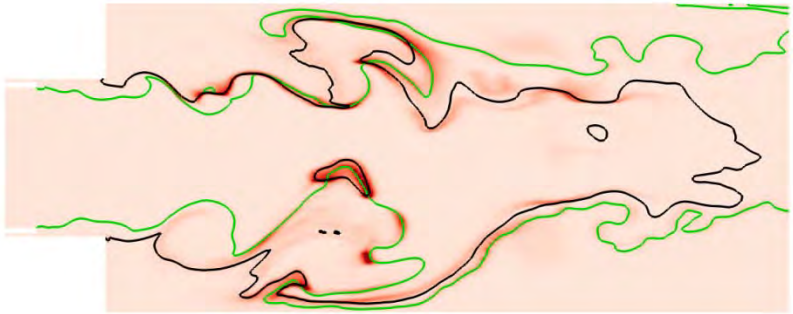

Heat Release – Take 2

LCM

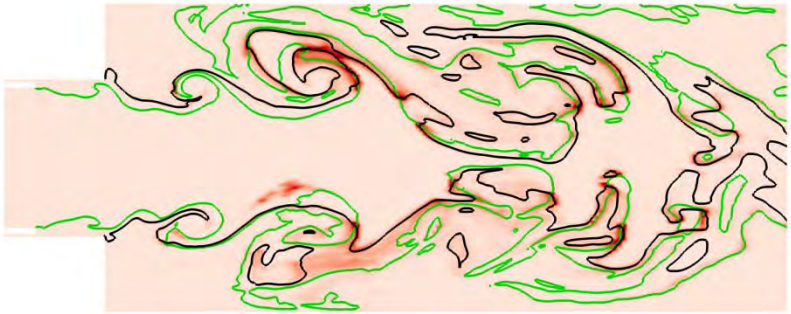

LEM

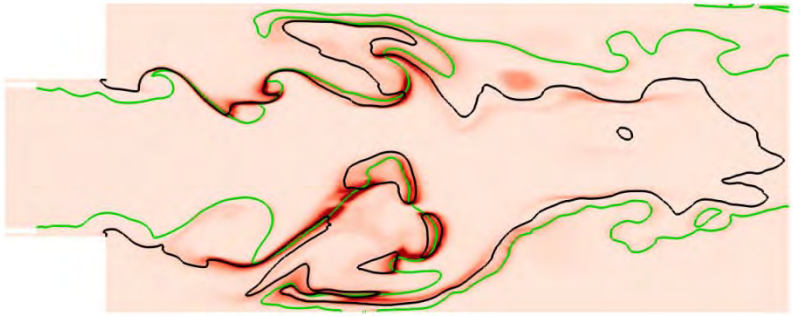

Unstable Operating Point

Second half of the heat release cycle. The LEM combustion initiates sooner resulting in more distributed combustion, less accumulated fuel and lower amplitudes.

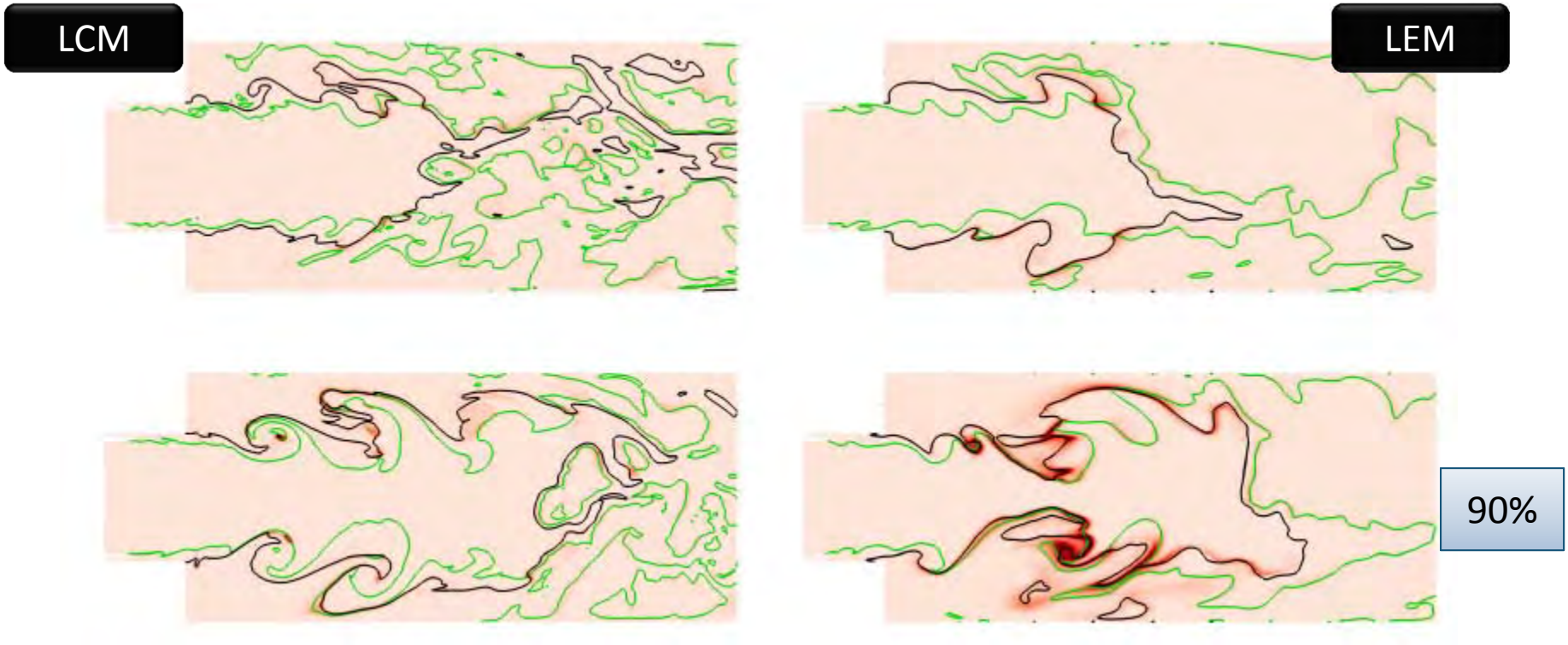

Fuel Cutoff

LCM

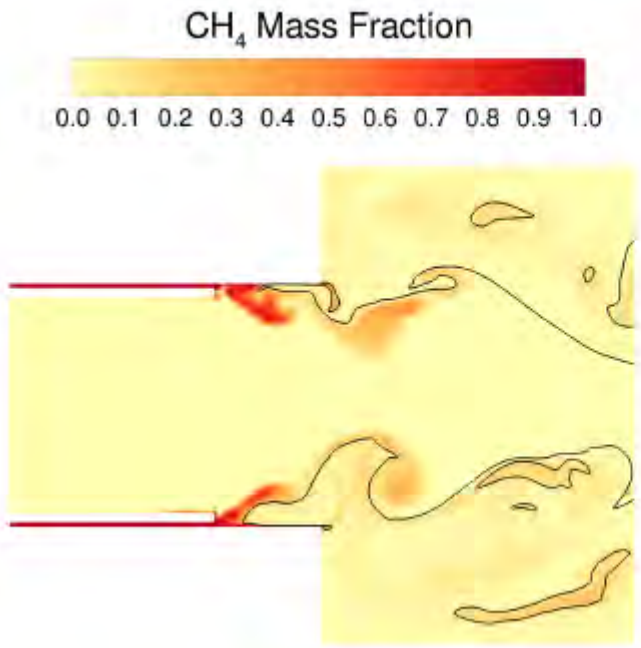

LEM

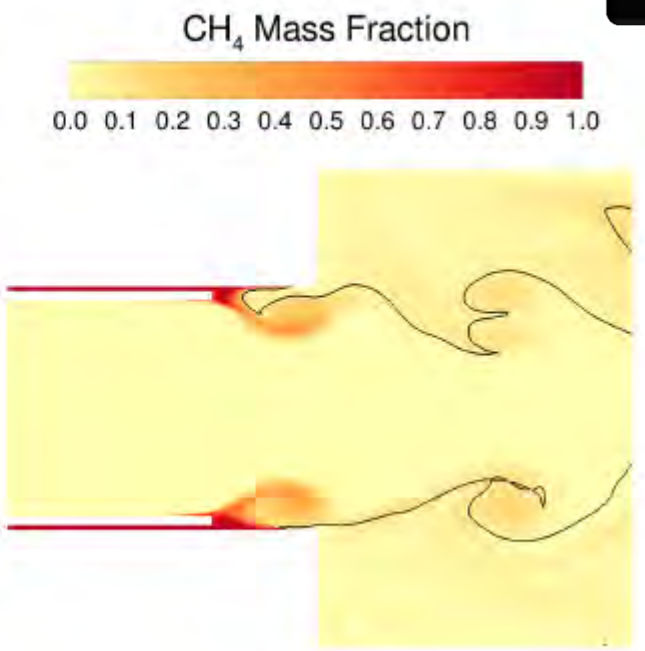

Fuel cutoff is captured by both simulations. More severe in the LCM simulation.

Fuel Cutoff

LCM

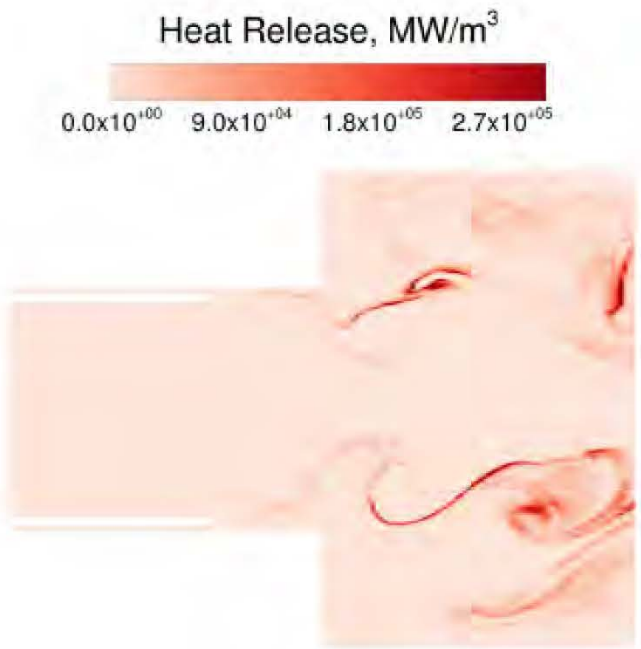

LEM

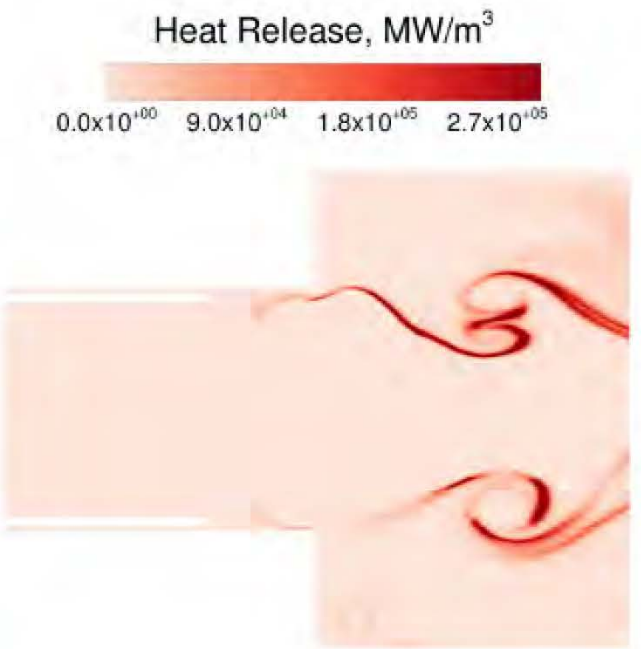

Both show heat release in the cup region during the fuel cutoff event.

Reignition

LCM

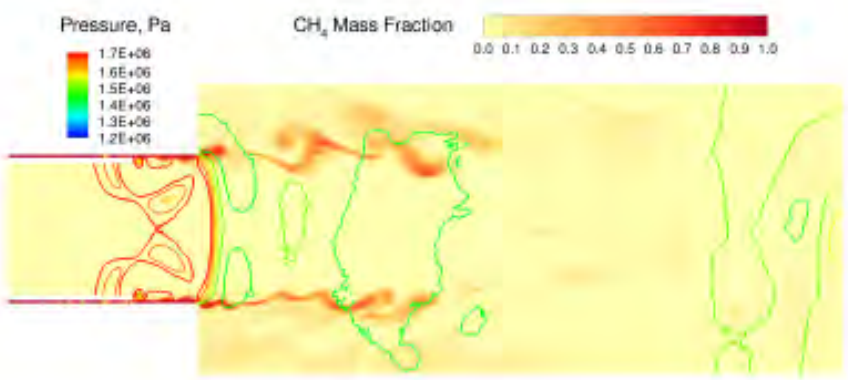

LEM

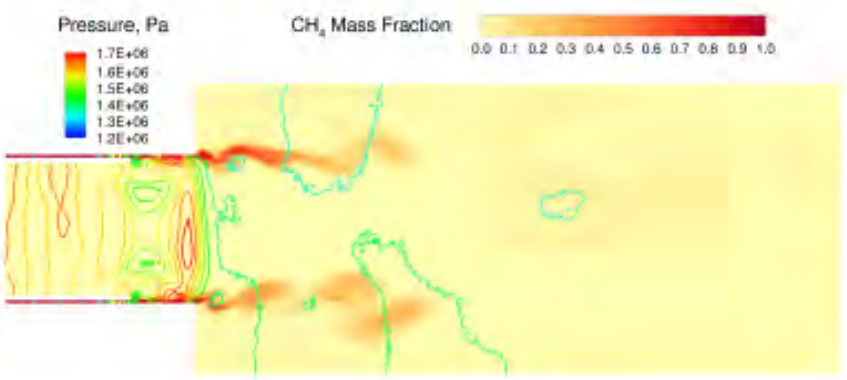

Large reignition event takes place due to the returning pressure wave in both simulations.

LCM shows less available fuel, especially in the reticulation region.

Summary

- The LEM has been applied to two combustion instability test cases and compared with companion simulations on identical meshes that used the LCM.
- The LEM is able to predict the marginally stable and unstable conditions correctly as is the LCM.
- The unstable LEM case becomes slightly **more stable**, while the marginally stable LEM case becomes somewhat **more unstable** than the LCM simulations.
- The LEM flowfield shows smoother flow features that are consistent with a thickened turbulent flame brush. The heat release is locally concentrated unlike in the LCM case, which shows a more distributed heat release pattern.
- The LEM simulation showed combustion slightly ahead of the acoustic events in the combustor.

Summary

- Improved LEM results over prior work.
- The present LEM results are not a significant improvement over the present LCM results.
- Some of the discrepancies may well be related to the limitations of the LEM model for finer grids.
  - Errors due to the lack of large scale species diffusion and the arbitrariness of the Lagrangian splicing may introduce errors.
- Further study including systematic grid resolution is necessary to elucidate these performance trends.

Computing resources were provided by the DoD High Performance Computing Modernization Program.